M.I.T. Plasma Science and Fusion Center Report #PSFC/JA-00-14
submitted to Nuclear Fusion June 2, 2000

# Cross-field plasma transport and main chamber recycling in diverted plasmas on Alcator C-Mod

B. LaBombard*, M.V. Umansky†, R.L. Boivin, J.A. Goetz, J. Hughes, B. Lipschultz, D. Mossessian, C.S. Pitcher, J.L. Terry, Alcator Group

*Massachusetts Institute of Technology, Plasma Science and Fusion Center, 175 Albany St., Cambridge, MA 02139 USA*

## Abstract

Cross-field particle transport increases sharply with distance into the scrape-off layer and plays a dominant role in the 'main-chamber recycling' regime in Alcator C-Mod, a regime where most of the plasma particle efflux recycles on the main-chamber walls rather than flows into the divertor volume. This observation has potentially important implications for a reactor: Contrary to the ideal picture of divertor operation, a tightly baffled divertor may not offer control of the neutral density in the main chamber such that charge-exchange heat losses and sputtering of the main chamber walls can be reduced.

The conditions that give rise to the 'main-chamber recycling' regime can be understood by considering plasma/neutral particle balance: When the flux-surface averaged neutral density exceeds a critical value, flows to the divertor can no longer compete with the ionization source and particle fluxes must increase with distance into the SOL. This critical neutral density condition can be recast into a critical cross-field plasma flux condition: particle fluxes must increase with distance into the SOL when the plasma flux crossing a given flux surface exceeds a critical value. Thus, the existence of the 'main-chamber recycling' regime is intrinsically tied to the level of anomalous cross-field particle transport.

Direct measurement of the effective cross-field particle diffusivities ($D_{eff}$) in a number of ohmic L-mode discharges indicates that $D_{eff}$ near the separatrix strongly increases as plasma collisionality increases. Convected heat fluxes correspondingly increase, implying that there exists a critical plasma density (~ collisionality) beyond which no steady-state plasma can be maintained, even in the absence of radiation.

---

*Tel.: 1-617-253-6942, Fax: 1-617-253-0627: e-mail: labombard@psfc.mit.edu.

†Laboratory for Laser Energetics, 250 East River Rd., Rochester, NY 14623 USA

Article Categories: I1,Te;F2,Te;J2,Te

## 1. Introduction

Magnetic divertors were originally conceived as a means for minimizing plasma-wall contact in the main chamber by redirecting the wall interaction to a chamber that is remote from the core plasma (fig. 1a). In this ideal picture, all particle and heat fluxes which cross the magnetic separatrix result in flows along open field lines to the divertor chamber. Volumetric heat dissipation in the divertor (radiation, charge exchange, recombination) reduces heat fluxes to target plates, impurities become trapped by entrainment in the plasma flow, and fuel gas plus helium ash is available at high neutral pressures for efficient pumping. It is often assumed that with sufficiently tight divertor baffling, neutral densities in the main chamber can be kept low such that charge-exchange heat losses from the core and sputtering of the main chamber walls can be controlled.

Experiments in Alcator C-Mod clearly demonstrate that this ideal picture of divertor operation does not universally apply [1]. Although the C-Mod divertor does receive most of the conducted and convected energy fluxes from the scrape-off layer (SOL) and does entrain/compress impurity and fuel gases, the divertor volume receives only part of the total particle efflux from the main chamber. Recycling in the main chamber scrape-off layer (MCSOL) is predominately onto surfaces in the main chamber and is large compared to the particle flow between the main chamber and divertor volumes (fig. 1b).

This ‘main-chamber recycling’ regime appears to be caused by two factors, the second of which may be fundamentally important for a reactor design: (1) The divertor structure in C-Mod is designed to be a tightly baffled one, optimized for high heat flux handling, not particle handling. It accommodates approximately one power e-folding distance over its vertical face. (2) Cross-field particle transport in the main chamber scrape-off layer increases markedly with distance from the separatrix, transporting plasma toward wall surfaces in the main chamber. In response, the radial density profile becomes nearly flat in the far scrape-off layer. This fundamental characteristic of the MCSOL transport is troublesome: There may be no practical way to design an 'ideal’ divertor for C-Mod that would accommodate the width of the particle flux profile in the MCSOL. Similar to

Alcator C-Mod, fusion reactors will employ a tightly baffled, heat-flux optimized divertor geometry and operate with wall surfaces that are fully saturated (i.e., with a unity particle recycling coefficient). Thus, the physics behind this regime of 'main chamber recycling' needs to be understood in a way that can be extrapolated to reactor conditions.

Evidence for increased cross-field particle transport in the far SOL and significant main-chamber recycling has been seen before in a number of other experiments. Similar to Alcator C-Mod [2], a 'shoulder' or a 'second e-folding length' in the cross-field density and temperature profiles have been seen in ASDEX [3] and JT-60U [4]. This feature is found to persist regardless of changes in the divertor geometry (ASDEX or ASDEX-U [5] and open or W-shaped divertor in JT-60U [6]). In ASDEX-U, the profiles in the shoulder region could be reproduced in simulations by assuming a large outward drift of 70 m $s^{-1}$ or an effective particle diffusion coefficient much larger than Bohm of $D_{eff} \sim 30$ $m^2$ $s^{-1}$ [3]. Also similar to results obtained on Alcator C-Mod [2, 7, 8], neutral pressures in the main chamber of ASDEX-U were unaffected in changing to a more closed divertor geometry (Div-I → Div-II) [9]. This result was anticipated from modeling the behavior of the Div-II divertor [10], owing the assumption that rapid transport in the far SOL would be independent of divertor geometry.

Main chamber recycling phenomena do not appear to be present to the same extent in all tokamaks. For example, DIII-D [11], JET [12], and JT-60U [4] report a reduction in main chamber ionization sources and neutral pressures, respectively, when the divertor was changed to a more closed geometry (adding outer baffle in the RDP-OB in DIII-D, going from Mk-I → Mk-IIA → Mk-IIAP in JET, and going from open to W-shaped divertor in JT-60U). This suggests that either a large level of main-chamber recycling is not occurring or it is sufficiently localized (at the divertor baffle, for instance) so that it does not set the midplane neutral pressures in these tokamaks.

In this paper, we investigate the physics of the 'main-chamber recycling' phenomenon in Alcator C-Mod, making use of an extensive array of particle balance measurements combined with

simple analytic modeling and detailed UEDGE simulations. Section 2 outlines the experimental arrangement and the operation of key diagnostics. Langmuir probes, $Ly_\alpha$ and $D_\alpha$ imaging systems, and neutral pressure measurement systems are described in some detail as they provided most of the results discussed in this paper.

Section 3 presents observations of global particle balance which clearly identify the regime of main-chamber recycling in Alcator C-Mod. Two principal characteristics emerge which are interrelated: (1) cross-field particle fluxes dominate over parallel fluxes in balancing the ionization in a given flux tube, and (2) effective cross-field particle diffusivities ($D_{eff}$) increase with distance from the separatrix. A simple particle balance model suggests that the regime arises when the flux-surface averaged neutral density near the separatrix exceeds a critical value. Equivalently, the regime will occur if the flux-surface averaged cross-field particle flux density exceeds a critical level. Thus, the existence of the main-chamber recycling regime appears to be connected more to the level of turbulent particle transport than to the details of the divertor geometry. To elucidate these and other ideas with a more complete physics model, results from 2-D edge plasma transport modeling [13] using the UEDGE code [14] are reviewed.

Section 4 describes results from local particle transport experiments. Effective cross-field particle diffusivity profiles ($D_{eff}$) are inferred directly from measurements using a local particle balance model. It is found that $D_{eff}$ increases strongly with distance from the separatrix, nearly identical to the results obtained from 2-D UEDGE simulations. The scaling of $D_{eff}$ with local parameters is examined, identifying collisionality as a potentially important parameter. Although these measurements were performed in low to moderate density plasmas, they suggest that there exists a plasma density (~collisionality) beyond which cross-field heat convection and charge exchange losses become too large for a steady-state plasma to exist. Finally, section 5 summarizes the key findings of this work.

## 2. Experimental Arrangement

All results reported in this paper were obtained in deuterium discharges with a diverted, lower single-null magnetic equilibrium, similar to that of fig. 2. In some discharges, a secondary separatrix can sometimes be present in the upper chamber. However, when this happens, the upper X-point occurs on field lines that map onto limiter surfaces in the main chamber. Results presented here are not sensitive to the upper X-point location in this regime. All discharges had plasma current ($I_p$) parallel to toroidal magnetic field ($B_T$) and had the $B x \nabla B$ ion drift directed towards the lower X-point. The geometry of the divertor and the arrangement of diagnostics for the present studies is also shown in fig. 2. Detailed information on Alcator C-Mod's design, diagnostics, and operational characteristics can be found elsewhere [15].

The plasma-facing surfaces in Alcator C-mod consist principally of molybdenum tiles with stainless steel or inconel support structures. Since January 1996, boronization of internal surfaces is performed at regular intervals. A mixture of 90% helium and 10% diborane is substituted for the fill gas in the electron-cyclotron discharge cleaning (ECDC) plasmas. In preparation for a day of running tokamak discharges, the wall is typically conditioned with ECDC deuterium or helium plasmas. However, the present conditioning techniques are found to have a small lasting influence on the inventory of active hydrogen isotopes in the wall: Following ~3 tokamak discharges, the gas-fueling behavior appears to return to the unconditioned-wall response. Thus, for almost all discharges, the first-wall in Alcator C-Mod can be considered to be ‘fully saturated’, i.e., having a global recycling coefficient near unity, with the specific value of the coefficient being determined by conditions in the few shots prior and the details of the present discharge (e.g., attempt at lower or higher density, RF heating, transitions to H/L mode).

The divertor structure is a baffled, ‘vertical plate’ design which is optimized to spread the power e-folding distance (1-4 mm, mapped to outer midplane) over the vertical portions of the divertor plates. A novel bypass valve system [7, 8] allows the neutral leakage from the divertor

volume to the main chamber to be controlled dynamically during a discharge. Primary limiter structures in the main chamber consist of a toroidally continuous inner-wall limiter, and principally two discrete outboard limiters spanning ~6 degrees toroidally and separated by ~180 degrees toroidally. The mid-section (~60 mm vertical section) of one of these limiters is toroidally displaced by ~40 degrees to accommodate diagnostic access. Secondary limiter structures exist ~5 mm (mapped to midplane) beyond the shadow of primary limiters at a number of toroidal locations. These are used to minimize plasma density at the surface of ICRF antennas which are in turn displaced another ~5 mm further into the SOL. The distance in major radius between the leading edges of the primary limiters and the outer wall is ~0.1 m at the midplane. This results in a relatively large poloidal conductance pathway for neutrals which recycle from outboard limiter surfaces. Typical values of the separatrix-to-limiter gaps for the data reported here were 15 to 18 mm (mapped to midplane), with inner and outer gaps similar. Scrape-off layer flux surfaces within this 15-18 mm band terminate either on the 'vertical' or 'horizontal' portions of the divertor structures.

Neutral pressures near the outer midplane are measured with two magnetically shielded gauges connected to the same pressure inlet (M, in fig. 2): (a) Bayard-Alpert ionization gauge ($10^{-9}$ – $10^{-3}$ torr) and (b) an absolutely calibrated baratron gauge ($10^{-4}$ – $10^{-1}$ torr). The overlapping pressure ranges of the two gauges allows the ionization gauge sensitivity to be checked. The inlet is positioned 10 cm toroidally from an outboard limiter. Consequently, it is possible that local recycling results in pressure readings that are larger than the toroidal average. Neutral pressures in the upper chamber (U, in fig. 2) and in the divertor are also measured with magnetically shielded, absolutely calibrated baratron gauges (upper chamber: $10^{-4}$ – $10^{-1}$ torr, divertor: $10^{-3}$ – 1 torr). Gas conductance pathways to the latter two gauges limit their time response to ~ 50 ms.

$D_\alpha$ light emission along radial chords passing through a point at the outer midplane and intercepting different vertical locations on the inner wall limiter is monitored by a photodiode array,

filtered to detect emission in a 10 nm band centered at 657.6 nm. For the present studies, the chords are located 30 cm toroidally from an outboard limiter and therefore may pickup a level of $D_\alpha$ emission that is somewhat higher than the toroidal average. However, $D_\alpha$ monitored at two other toroidal locations during previous run campaigns has yielded comparable signals (within a factor of 2) under the same discharge conditions. This indicates that either toroidal asymmetry contributions are small or that the dominant contribution to the $D_\alpha$ signal comes from recycling at the inner-wall limiter surface. Absolutely calibrated brightnesses from radial chords which span a vertical extent of 0.1 m about the vertical plasma center are of particular interest for the present studies.

Profiles of $Ly_\alpha$ emission across the outer scrape-off layer are detected along 20 chords which view tangentially to magnetic flux surfaces (see fig. 2). An array of extended spectral response VUV diodes, mounted in vacuum behind a narrow bandpass filter, receives light in a 7.6 nm band centered at 121.5 nm. Using a simple Abel inversion algorithm, the absolutely-calibrated chordal brightnesses yield a cross-field $Ly_\alpha$ emissivity profile with 2 mm spatial resolution [16]. The chords become tangent to magnetic flux surfaces at a location that is separated 30 cm toroidally from an outboard limiter, corresponding to the location of the $D_\alpha$ chords described above. Since chord-integrated atomic deuterium densities are small ($nL < 10^{17}$ $m^{-2}$) corrections due to $Ly_\alpha$ absorption and scattering are presently neglected [17].

High resolution profiles of electron temperature and density across the separatrix are obtained from an edge Thomson scattering system [18]. The laser scattering volumes are located in the upper chamber region (fig. 2). In the discharges presented here, this system provided 8 to 10 data points over a profile from 8 mm inside to 3 mm outside the separatrix, mapped to the midplane.

Electron density and temperature profiles in main-chamber scrape-off layer up to the separatrix are measured with two scanning probe systems (fig. 2): a vertical-scanning probe that samples plasma at a position 'upstream' from the entrance to the outer divertor, and a horizontal-scanning probe that records plasma conditions 10 cm above the midplane. Both probes employ a

molybdenum head with four tungsten Langmuir probe elements. The probe elements have directional sensitivity (along and across *B*), maintain a field line grazing angle of about 20 degrees, and project a current-collecting area with dimension transverse to flux surfaces of ~0.5 mm mapped to the midplane. Densities and temperatures along the probe's trajectory are obtained every 0.25 msec (corresponding to ~0.25 mm of probe travel) by fitting positive and negative-going *I-V* characteristics generated by a 2 kHz voltage sweep. Two of the probe elements in each scanning probe system can be used to form a 'Mach probe' in which the plasma flow parallel to the local magnetic field can be estimated from the ratio of ion saturation currents [19]. Cross-field profiles of both parallel and *ExB* flows can be inferred with the scanning Mach probes. By integrating the poloidal projection of these flows along the trajectory of the vertical scanning probe, the particle flux directed towards the outer divertor throat and baffle structure can be obtained.

Langmuir probes are mounted on both the inner and outer divertor plates at 16 poloidal locations. The probes consist of tungsten elements, extending 0.5 mm beyond the surface and having a 10 degree angle with respect to the divertor surface. Plasma density, temperature, and ion flux profiles across the divertor surface are deduced at roughly 10 msec intervals by fitting current-voltage characteristics using standard magnetized probe theory.

Cross-field profile data from all diagnostics are mapped onto magnetic flux surfaces reconstructed from magnetic measurements [20] and the EFIT plasma equilibrium code [21]. Flux surfaces in the scrape-off layer are labeled by the coordinate $\rho$, which is defined as the distance in major radius outside the last-closed flux surface at the outboard mid-plane. The electron stagnation pressure profiles measured by the divertor probes, the scanning probes and the edge Thomson scattering system can be made to overlay by adjusting their relative flux surface mappings in $\rho$. The technique is employed in this paper, to 'align' the data from these diagnostics. Flux-surface mapping corrections ($\Delta\rho$) range from 0 to 8 mm, which can exceed the expected accuracy of the EFIT reconstruction and the positioning accuracy of the diagnostics. Possible sources for errors are

being presently being explored. Fortunately, the principal results presented in this paper (e.g., main-chamber recycling fluxes, $D_{eff}$ profiles) are not sensitive to mapping corrections. For example, $D_{eff}$ profiles (section 4) are deduced from horizontal scanning probe and tangential $Ly_\alpha$ data, with known major radii. Consequently, these estimates of $D_{eff}$ are insensitive to uncertainties in determining which flux surface should be labeled as the separatrix surface.

## 3. Main-Chamber Recycling Regime in C-Mod

Wall-recycling clearly dominates the fueling of the main-chamber scrape-off layer in Alcator C-Mod. Although recycling on the divertor baffle plate is large, recycling on the limiter/wall structures surrounding the core plasma is even larger, comparable to the recycling inside the divertor volume. Even a crude analysis of global particle balance using neutral pressure measurements and $D_\alpha$ light emission clearly reveals the phenomenon. All plasmas studied to date appear to exhibit this behavior.

### *3.1. Global Particle Balance*

Fig. 3 shows neutral pressures at the divertor, upper chamber, and midplane locations as a function of line-averaged electron density ($\bar{n}_e$) in otherwise identical discharges ($I_p$ = 0.8 MA, $B_T$ = 5.3 tesla, ohmic L-mode, $1.0\text{x}10^{20}$ m$^{-3}$ < $\bar{n}_e$ < $2.3\text{x}10^{20}$ m$^{-3}$). These discharges span the parallel heat transport regimes of the outer divertor leg, documented previously [2]: low recycling or sheath-limited heat transport regime ($\bar{n}_e < 1.4 \text{ x } 10^{20}$ m$^{-3}$), high recycling divertor regime ($1.4\text{x}10^{20}$ m$^{-3}$ < $\bar{n}_e$ < $2.1\text{x}10^{20}$ m$^{-3}$) and detached regime ($\bar{n}_e > 2.1\text{x}10^{20}$ m$^{-3}$). Typical plasma densities at the divertor plate span the range $10^{20}$ m$^{-3}$< $n$ < $10^{21}$ m$^{-3}$with electron temperatures in the range of 3 < $T_e$ < 40 eV. Detailed information on the divertor plasma conditions for these discharges can be found in [2]. Note that while the neutral pressures in the main chamber are a factor of 100 or more

lower than in the divertor, they can be quite high (0.03 – 2 mtorr). Also, note that the upper chamber pressure is always a factor ~ 3 or more higher than the midplane pressure. If main-chamber recycling were absent or if main-chamber recycling was restricted to the top of the divertor baffle, one would expect the neutral pressure in the upper chamber to be much lower than the midplane, yet the opposite is true. The higher pressure in the upper chamber may in part be explained by the existence of an upper secondary X-point in the far scrape-off layer which could result in some compression of neutrals. In any case, it appears that high neutral pressures surround the core plasma in the main chamber.

Data points in fig. 3 with open symbols correspond to discharges in which the divertor bypass flaps [7, 8] were open. Under these conditions, the leakage conductance pathway from the divertor volume to the main chamber is approximately doubled. Fig. 3 shows that the divertor neutral pressure correspondingly drops by a factor of ~2 for $n_e > 1.3 \times 10^{20}$ m$^{-3}$. Yet, the midplane and upper chamber pressures are not affected at all.

One can crudely estimate the flux of atomic neutrals attacking the main-chamber plasma from these pressure measurements. In steady-state, the flux of neutrals entering and exiting along the pipes connected to the pressure gauge volumes must balance. If we assume that the exiting flux is a free molecular flow of deuterium at the wall temperature, then the local molecular flux density heading back towards the plasma is readily computed. Once the molecules encounter the SOL plasma, they rapidly undergo Franck-Condon dissociation where approximately half of the resulting atomic deuterium proceeds further into the plasma. Assuming that this flux density is uniform over the area of the main chamber plasma (~ 7 m$^2$), one arrives at an estimate for the atomic flux from the wall, $\Gamma_w$, based on the neutral pressure at the wall, $P_w$,

$$\Gamma_w \ (\text{s}^{-1}) \approx 8\text{x}10^{22} P_w \ (\text{mtorr}). \qquad (1)$$

From this estimate we see that poloidally averaged neutral pressures in the range 0.03 – 2 mtorr imply main-chamber fueling rates that are quite large, of order $10^{21}$ – $10^{23}$ $s^{-1}$. (Note: at high neutral pressures, neutral-neutral collisions render eq. (1) less reliable. Section 4 examines the validity of eq. (1), using experimental data. Also note that eq. (1) is only appropriate for estimating the neutral fluxes at the midplane. Neutral fluxes and pressures in the divertor are related in a more complicated way, involving momentum transfer between the plasma/neutral species.)

Fig. 4 shows estimates of ionization source in the main chamber ($S_{ion}$), ion flux arriving on the divertor plates ($\Gamma_{div}$), and ion flux heading towards the divertor ($\Gamma_{throat}$), as a function of atomic flux from the wall, ($\Gamma_w$), for the same set of discharges as shown in fig. 3. The fluxes (in units of $s^{-1}$) were estimated as follows:

- $\Gamma_w$ is evaluated from eq. (1) using the midplane neutral pressures in fig. 3.
- $S_{ion}$ is obtained from $D_\alpha$ brightness ($B_\alpha$) from a midplane chord (see fig. 2) assuming 45 ionizations per $D_\alpha$ photon [22] and assuming poloidally uniform emissivity over a narrow shell at the separatrix, $S_{ion}$ ($s^{-1}$) ≈ $6x10^{21}$ $B_\alpha$ (W $m^{-2}$ $ster^{-1}$).
- $\Gamma_{div}$ is obtained by integrating the ion flux density profiles over the surface of the inner and outer divertor structure, including the divertor baffles. In cases where the complete profile across the inner divertor is not measured (bad data), the inner divertor flux is scaled relative to that of the outer divertor from discharges of similar density.
- $\Gamma_{throat}$ is an estimate of the plasma flux heading toward the throat of the divertor and the divertor baffle structure from the MCSOL. It is evaluated as twice the integral of the poloidal flux density directed towards the divertor structures at the vertical scanning probe location arising from the vector sum of *ExB* and parallel flows. The integral is performed over an area defined by the trajectory of the probe (see fig. 2), revolved around the torus centerline. For these discharges, *ExB* flows in the outer leg are directed towards the outer

divertor. On the inner leg, the *ExB* component of the flow is likely to be away from the divertor. Thus this may be considered as an upper bound estimate of the flux.

Even allowing for possible factors of ~2 errors in the estimated fluxes, Fig. 4 clearly illustrates that main-chamber recycling dominates the MCSOL particle balance in Alcator C-Mod over a density range that includes sheath-limited, high-recycling, and detached divertor regimes. Flux toward the divertor structures is always less than 1/4 of the ionization source in the main chamber as inferred by $D_\alpha$ measurements. Moreover, the recycling in the main chamber is comparable (based on $\Gamma_w$ estimate) or even greatly exceeds (based on $S_{ion}$ estimate) the recycling on the divertor surfaces! Thus, while a strong level of recycling occurs in both the divertor and main chamber volumes there appears to be a relatively weak flux of particles communicating between them.

The fact that $S_{ion}$ and $\Gamma_w$ in fig. 4 have a dramatically different slope and only agree at high plasma density (or wall flux) is also interesting. It is possible that $B_\alpha$ includes contributions from reflected light from the inner wall or recombination radiation leading to an overestimate of $S_{ion}$. However, preliminary measurements of $Ly_\alpha$ emissivity profiles on the small major radius side of the plasma support a more likely explanation:[23] recycling on the inside of the torus (i.e., inner limiter) is more intense than on the outside. Thus, the poloidal distribution of neutral pressure may in fact be *minimum at the outer midplane*. An implication of figs. 3 and 4 is that as the plasma density is increased, the neutral pressure surrounding the plasma becomes more uniform.

### *3.2. Conditions for Main Chamber Recycling Regime*

#### *3.2.1. A critical flux-surface averaged neutral density*

The above observations indicate that ionization sources in the MCSOL are balanced primarily by cross-field particle fluxes extending all the way onto the far SOL and arriving 'locally' on main-chamber wall surfaces. Although parallel flows in the MCSOL are undoubtedly present,

they appear to be of secondary importance. The essential physics in this regime can be most readily understood by analyzing particle balance in a highly simplified SOL. Conservation of plasma and neutral species requires

$$\nabla\Gamma = n_0 n k_{ion} \tag{2}$$

$$\left(\Gamma + \Gamma_0\right) = 0 \tag{3}$$

where $\Gamma$ and $\Gamma_0$ are the plasma and atomic neutral fluxes, $n$ and $n_0$ are the corresponding densities and $k_{ion}$ is the ionization rate coefficient. Here, we assume that contributions from molecular species and volume recombination can be neglected in the region of interest. The SOL plasma can be decomposed into a series of adjacent flux tubes, each with length $2L$, extending from one axisymmetric divertor surface to the other. For the purpose of illustration and the desire of simplicity, we consider the case when electron temperatures and densities are nearly constant along the flux tubes and the divertor surfaces are locally perpendicular to poloidal flux surfaces. Given that the main-chamber recycling condition is seen to persist in both sheath-limited and high recycling divertor regimes, the former restriction apparently does not exclude the essential physics. As a consequence of the orthogonal flux surface/wall geometry, the divertor plate becomes a flat, horizontal surface with no baffle structure. We may consider it as approximating a 'virtual divertor surface' formed by the divertor throat plus the baffle structure in the actual geometry of C-Mod.

Averaging (<...>) eqs. (2) and (3) over a flux surface bounded by the wall, one obtains

$$\frac{\partial}{\partial x}\langle\Gamma\rangle = n\left(\langle n_0\rangle k_{ion} - \frac{C_s}{2L}\right) \tag{4}$$

$$\frac{\partial}{\partial x}\langle\Gamma\rangle + \frac{\partial}{\partial x}\langle\Gamma_0\rangle = 0 \tag{5}$$

where the sheath density is approximated as 1/2 the nominal density in the flux tube, $n$, the parallel flow to the surface is at the sound speed, $C_s$, and the cross-field (i.e., across flux surface) metric,

$x$ , is approximated to be independent of the parallel coordinate. Equation (5) makes use of unity recycling on the divertor surface, i.e., the parallel flux of ions projected onto the surface-normal of the divertor balances the flux of neutrals leaving that surface. Stated another way, eq. (5) says that the average plasma flux density crossing any closed magnetic flux surface or magnetic flux surface terminating on an axisymmetric wall perpendicular to $B_0$ must be balanced (to within a constant offset) by an oppositely directed average neutral flux density. Conservation of mass in the closed volume requires this constant offset to be zero so that,

$$\langle \Gamma \rangle = -\langle \Gamma_0 \rangle . \qquad (6)$$

Now consider what happens to the average flux density of plasma passing through a given magnetic flux surface. Equation (4) shows that this flux will decrease with distance into the SOL if the flux-tube averaged ionization source does not exceed the losses from parallel flow towards the divertor surface. However, if the flux-tube averaged neutral density, $\langle n_0 \rangle$, exceeds some critical density, $\langle n_0 \rangle_{crit}$, then $\langle \Gamma \rangle$ *increases* with distance into the SOL. Note that if $\langle \Gamma \rangle$ increases with distance into the SOL then one would expect $\langle n_0 \rangle$ to also increase with distance into the SOL, since in this case the overall recycling level is increasing with distance into the SOL. Thus, if $\langle n_0 \rangle_{crit}$ is exceeded at *some location* in the SOL then it will most likely be *exceeded at all locations farther into the SOL* up to the point where $C_s / L$ increases sufficiently, e.g., at the location of a limiter surface. Therefore, this model suggests the following picture: When the flux-surface averaged neutral density near the last-closed flux surface is on the order of $\langle n_0 \rangle_{crit}$, the ionization source in the *entire* SOL becomes balanced primarily by cross-field fluxes, the cross-field flux increases all the way out to the nearest main chamber surface (limiter, antenna,…), and we have a MCSOL that exhibits main-chamber recycling dominated behavior.

Note that the physical separation between the last-closed flux surface and the main chamber limiter/wall does not appear in this analysis. Even if the walls where infinitely far away, this analysis would still lead to main-chamber recycling behavior for $\langle n_0 \rangle > \langle n_0 \rangle_{crit}$ near the separatrix. In this case, the poloidal distribution of ion fluxes on the main-chamber walls would no doubt change, favoring the highest plasma and neutral fluxes near the divertor baffle structure. Still, $\langle \Gamma \rangle$ and $\langle n_0 \rangle$ would increase with distance into the SOL. At some location in the far SOL, volume recombination would occur, effectively playing the role of a wall surface.

*3.2.2. A critical cross-field particle flux density*

In this simple SOL, we can relate the critical neutral density, $\langle n_0 \rangle_{crit}$, to a critical cross-field plasma flux density, $\langle \Gamma \rangle_{crit}$, by making use of eq. (6). The maximum neutral flux density that can arise from a specified local neutral density is the 'free-streaming' value: $\Gamma_0 \leq n_0 \overline{v_0}$ where $\overline{v_0}$ is the average velocity of neutrals heading in the direction of $\Gamma_0$. If we assume that via charge exchange, the neutral distribution is approximately maxwellian with a temperature that is roughly equal to or lower than the local ion temperature ($T_i$), then we can compute a minimum neutral density required to support the local neutral flux density,

$$n_0 \geq \Gamma_0 \sqrt{\frac{2\pi\, m_D}{kT_i}} \quad . \tag{7}$$

Now, from eq. (6), we find that there exists a critical cross-field *plasma* flux density, above which $\langle n_0 \rangle$ must exceed $\langle n_0 \rangle_{crit}$,

$$\langle \Gamma \rangle_{crit} = \frac{C_s}{2\, Lk_{ion}} \sqrt{\frac{kT_i}{2\pi\, m_D}} \, . \tag{8}$$

With $T_i \approx T_e$, $k_{ion}$~ 2x10$^{-14}$ m$^3$ s$^{-1}$, and relating the connection length to safety factor (*q)* and major radius (*R*), $L \approx \pi\, qR$, eq. (8) becomes,

$$\langle \Gamma \rangle_{crit} \approx 2x10^{20} \frac{T(eV)}{q\,R(m)} \quad (m^{-2}s^{-1}). \qquad (9)$$

Thus, the regime of main-chamber dominated recycling is *intrinsically dependent on the level of anomalous cross-field plasma transport* in the MCSOL.

We must keep in mind that the model outlined here is grossly over-simplified. Large density gradients and pressure gradients (e.g., detachment) routinely exist along open field lines with $T_i \neq T_e$. Recombination can contribute or dominate the particle balance in the divertor. Divertor plates are typically inclined with respect to flux surfaces. Molecules contribute to the particle balance and the neutral energy distributions are far from a Maxwellian evaluated at the local ion temperature. Nevertheless, the plasma and neutral species still must satisfy mass balance. Thus, the essential result from the above model must still hold: For any flux surface in the SOL, there must exist some critical value of $\langle \Gamma \rangle$ (or equivalently $\langle n_0 \rangle$) such that at locations further out into the SOL the cross-field plasma fluxes dominate the flux-tube particle balance. In the case when the critical $\langle \Gamma \rangle$ is achieved near the last-closed flux surface, then the entire SOL can have radially-dominated transport resulting in the regime of main-chamber recycling. Whether and where critical $\langle \Gamma \rangle$ values are achieved in a given discharge depends heavily on the details of the cross-field plasma transport.

Although the above model is clearly a qualitative one, it is entertaining to compare the order of magnitude estimate of $\langle \Gamma \rangle_{crit}$ from eq. (9) with the fluxes shown in fig. 4. For values of $T$ ~ 50 eV, $q$ ~ 4, and $R$ ~ .67 m, $\langle \Gamma \rangle_{crit}$ times the area of the last-closed flux surface is ~ 3x10$^{22}$ s$^{-1}$. It is

interesting that the fueling rates of the MCSOL inferred from $D_\alpha$ approach or exceed this value for all the discharges shown in fig. 4.

*3.2.3. Why doesn't the MCSOL density profile in C-Mod have negative curvature?*

Reviewing published results on many tokamaks, it appears that cross-field density profiles in the main-chamber scrape-off layer always fall off more or less exponentially with distance from the last-closed flux surface, i.e., the second derivative (curvature) of the cross-field density profiles is always positive. This observation also holds true for all discharges studied to date in Alcator C-Mod, even though the plasmas exhibit large main-chamber recycling, as shown in fig. 4. Note that if one looks at the cross-field density profile alone, one can be mislead to conclude that main-chamber recycling is *not* occurring and that the divertor *is* receiving almost all of the particle efflux. For a number of years, this was the naïve interpretation of the particle balance situation in Alcator C-Mod. Equation (4) allows us to examine the root cause of this misinterpretation.

Consider the definition of an effective particle diffusion coefficient, $D_{eff}$, such that the cross-field particle flux satisfies

$$\Gamma = -D_{eff} \nabla n, \tag{10}$$

and eq. (4) becomes

$$\left\langle D_{eff} \frac{\partial^2 n}{\partial x^2} \right\rangle + \left\langle \frac{\partial D_{eff}}{\partial x} \frac{\partial n}{\partial x} \right\rangle = -n \left[ \langle n_0 \rangle k_{ion} - \frac{C_s}{2L} \right]. \tag{11}$$

If one *assumes* that $D_{eff}$ is approximately constant in space, then one expects the density profile to have positive curvature (i.e., $\partial^2 n / \partial x^2 > 0$) when divertor flows dominate and *negative curvature* ($\partial^2 n / \partial x^2 < 0$) *when main-chamber recycling dominates.* Density profiles with negative curvature are typically present just inside the last closed flux surface where, by definition, flow to the divertor is zero. Thus, in seeing density profiles with positive curvature, one could erroneously conclude that all the plasma efflux is going to the divertor (or at least the divertor plus baffle plate structure), i.e.,

the divertor is operating as an ideal divertor. Clearly, the problem is in assuming that $D_{eff}$ is constant. In fact, we now know that $D_{eff}$ varies so strongly with distance into the C-Mod SOL that the second term in eq. (11) is the most important one in setting the curvature of the density profile in the far SOL.

Fig. 5 shows results from UEDGE modeling of two ohmic L-mode discharges [13] with conditions otherwise similar to those shown in fig. 4. ($I_p$ = 0.8 MA, $B_T$ = 5.3 tesla): a high midplane neutral pressure case with $n_e$ = 2.4 x $10^{20}$ $m^{-3}$, $P_{mid}$ = 0.3 mtorr, and a low midplane pressure case with $n_e$ = 1.2 x $10^{20}$ $m^{-3}$, $P_{mid}$ = 0.025 mtorr. Density profile data points are obtained from the vertical scanning probe and they show the persistent positive curvature in the SOL. In order to match both the density profile shape and the neutral pressures measured in the main chamber, it is necessary to have $D_{eff}$ increasing rapidly with distance from the separatrix, as shown. Owen [24, 25] has independently modeled the scrape-off layer plasma and neutral transport in Alcator C-Mod using B2.5 coupled with DEGAS. The conclusions are the same: cross-field fluxes must remain high or increase with distance from the separatrix. Since the density profile becomes flatter with distance from the separatrix, this necessitates postulating an outward radial velocity that increases with distance into the SOL.

Recently, experiments aimed at characterizing the cross-field transport behavior of helium in the scrape-off layer have been performed in Alcator C-Mod [26]. The ratio of singly- to doubly-charged $^3$He ions arriving at the wall was measured directly with an ion mass spectrometer. It is found that in order to account for the relatively small proportion of doubly-charge ions arriving at the wall, the cross-field diffusive and/or convective transport of helium must increase with distance from the separatrix. Far in the SOL, the magnitude of the effective particle diffusion coefficients exceed the Bohm level by more than two orders of magnitude, implying that an outward convection model is a more appropriate description.

It should be noted that evidence for effective cross-field *heat diffusivity* ($\chi_{eff}$) increasing with distance into the SOL has been seen before in 'onion-skin' modeling of JT-60 [27], JET [28, 29], and C-Mod [30]. A question naturally arises as to whether cross-field *heat convection* can become the dominant player in the SOL power balance. As discussed in the next section, when main-chamber recycling is large, both cross-field convection and charge exchange energy losses can dominate the local power balance, making extraction of the heat conduction component of $\chi_{eff}$ impractical.

### *3.3. UEDGE Simulation of Main Chamber Recycling in C-Mod*

Further insight into main-chamber recycling physics can be gained by examining the output from UEDGE simulations [13] of two ohmic L-mode discharges in more detail. The computational domain, employing a locally orthogonal mesh and a wall surface that approximates that of Alcator C-Mod, is shown in fig. 6. The orthogonal mesh is seen to adequately describe the region of interest here which is the scrape-off layer outside the divertor volume. The specific details of transport and recycling within the C-Mod divertor volume is not addressed in this model. The cross-field profile of $D_{eff}$ was adjusted in each case so as to yield a match with the measured density profile (fig. 5). A spatially constant value of $\chi_\perp$ ($=\chi_{i\perp}=\chi_{e\perp}$) with range $0.1 < \chi_\perp < 0.5$ $m^2$ $s^{-1}$ was chosen to provide a match with the electron temperature profiles. However, owing to the role of heat convection and charge exchange energy losses (discussed in more detail in section 3.3.2) the modeled profiles are not sensitive to the specific value of $\chi_\perp$.The recycling coefficient on all wall surfaces was set to unity, requiring the boundary condition that the local plasma flux density to the wall balances the local neutral flux density from the wall. The midplane pressures were matched to within 25% of experiment.

*3.3.1. Particle Balance*

It is convenient to divide the plasma into four regions, as shown in fig. 6: Core Plasma, Main SOL, X-pt SOL, and Divertor. In this arrangement, the Langmuir/Mach probe flow measurements are located near the interface between the X-pt and Main SOL regions. The communication of plasma and neutral fluxes between these regions is shown in fig. 7. The width of the arrows within each case are proportional to the fluxes. The numerical values indicate the magnitude in units of $10^{21}$ $s^{-1}$.

Fig. 7 clearly illustrates the 'main-chamber recycling' behavior of the C-Mod MCSOL and its persistence despite an order of magnitude change in $P_{mid}$ and a corresponding factor of 30 change in the plasma fluxes on the MCSOL wall:

- The plasma flux from the Main SOL to the Wall always exceeds the plasma flux from the Core Plasma to the Main SOL. In case (b), the cross-field plasma flux amplification is greater than a factor of 2.
- Plasma flow from the Main SOL to the X-pt SOL is always less than the flux from the Main SOL to the Wall. For the low $P_{mid}$ case it is 1/2 of the wall flux while in the high $P_{mid}$ case it is 1/4 of the wall flux.
- The relative contribution to core fueling of Main and X-pt SOL neutrals remains remarkably constant over the factor of 10 change in $P_{mid}$. The Main SOL contributes 38% and 40% of the core fueling for the low and high $P_{mid}$ cases, respectively.
- The relative level of wall-recycling around the X-pt region changes strongly in going from the low to high $P_{mid}$ case. Apparently, at high $P_{mid}$ the flow towards the divertor is low enough and the cross-field transport is high enough to cause even the X-pt region to recycle as much on the wall as it does with the divertor volume.

The fluxes from the UEDGE simulations can be compared to the fluxes estimated directly from experimental data (fig. 4) in similar discharges. The open diamonds in fig. 4 show the total ionization in the main chamber from the UEDGE simulation (X-pt + Main SOL + Core contribution) while the open star symbols indicate the plasma flux from X-pt → Divertor regions, simulating the Mach probe measurement. As in the experimental data, the horizontal axis for these points is evaluated from the midplane neutral pressure via eq. (1). The UEDGE simulations are seen to match the key experimental findings: The trend with $P_{mid}$ is clearly reproduced and the flow directed towards the divertor is always much lower that the main chamber ionization flux. The discrepancy with the $D_\alpha$-inferred main chamber ionization at low $P_{mid}$ is perhaps explained by a persistent level of recycling on the inner limiter surface which is not included in the UEDGE simulation.

*3.3.2. Cross-field heat transport*

The high level of cross-field plasma convection in these plasmas has important consequences for heat transport through the separatrix and across the SOL. As shown in fig. 8, the cross-field heat flux profiles from the two UEDGE simulations can be decomposed into the following 4 principal contributions:

(a) Anomalous Plasma Heat Conduction ($\chi_a = \chi_{i\perp} = \chi_{e\perp}$)

$$q^{cond} = -n\chi_a \quad (T_i + T_e)$$

(b) Electron Convection

$$q_e^{conv} = \frac{5}{2} T_e n V$$

(c) Charge Exchange

$$q^{cx} = -n\chi_{cx} \quad T_i$$

(d) Ion plus Neutral Convection

$$q_{i+n}^{conv} = \frac{5}{2} nT_i V + \frac{5}{2} n_0 T_0 V_0 \quad .$$

Here $nV$ and $n_0 V_0$ are cross-field plasma and neutral fluxes, respectively. Since these fluxes nearly balance locally and $T_0 \sim T_i$ , the net heat flux contribution from (d) is small. In computing (c), we have used a diffusion approximation which breaks down (i.e., leads to an over-estimate) when the charge exchange mean-free path becomes comparable to the temperature gradient scale length. However, simulations with a flux-limiting factor yield similar results [13].

Fig. 8 shows the cross-field heat flux profiles arising from the above 4 processes, integrated over the local flux surface area and plotted versus radial distance from the separatrix at the outer midplane ($\rho$). The impact of main-chamber recycling on the heat transport channels is clear: Charge exchange and electron heat convection can play a significant role. Only in the low $P_{mid}$ case does anomalous plasma heat conduction set the magnitude of the transport level in the SOL, and only within a few millimeters of the separatrix! Charge exchange always appears to be a player, particularly in the far SOL. At high $P_{mid}$, electron convection becomes the key component over the entire SOL.

These observations underscore the complexity of cross-field heat transport processes in the SOL and the ambiguity that arises in assigning a single transport parameter, e.g. $\chi_{eff}$, to the transport behavior. One might expect that in the moderate to low $P_{mid}$ cases, $\chi_{eff}$ in the far SOL would be more of an indication of $\chi_{cx}$, while in high $P_{mid}$ cases, $\chi_{eff}$ would be set by $D_{eff}$ and the ratio of the temperature to density gradient scale lengths. It is interesting to note that using scrape-off layer profile data from Alcator C-Mod and JET, Connor et al. [31, 32] identified charge exchange as being a leading-candidate theoretical model for explaining the scrape-off layer width

scalings. Perhaps a different conclusion would be obtained using C-Mod data in a restricted data set where $\chi_a$ dominates the transport (e.g., for locations near separatrix at moderate to low $P_{mid}$).

Finally, note that in contrast to the particle balance picture, fig. 8 indicates that most of the energy entering into the SOL flows towards the divertor. Only, about 1/5 to 1/4 of the power in the SOL leaves through the wall boundary. Thus while the divertor is non-ideal with regard to the particle efflux, it is close to ideal with regard to receiving all of the power efflux (minus radiation) from the core plasma.

**4. Local Particle Transport Measurements in MCSOL**

In contrast to the cross-field heat transport picture, cross-field particle transport analysis is actually made easier by the main-chamber recycling phenomenon. In the case when the divergence of the parallel flows are of secondary importance, the local cross-field flux densities can be estimated by simply integrating the local cross-field ionization source profile. Here we employ this procedure, making use of the measurements of $Ly_\alpha$ emissivity, plasma density and electron temperature profiles across the separatrix and into the SOL. Profiles of cross-field particle flux density and $D_{eff}$ are thereby obtained and the scaling of local $D_{eff}$ is examined. The sensitivity of the results to the magnitude of parallel flows is parameterized and quantified by UEDGE modeling results (discussed above) and measurements of fluxes towards the divertor from the Mach probe. In addition, plasma fluxes onto the outboard limiter are inferred from probe measurements. The latter measurements are used to verify that the particle flux arriving at the main-chamber limiter/wall surface approximately balance the local ionization source deduced from $Ly_\alpha$ emissivity measurements.

*4.1. Local Particle Balance*

*4.1.1. Model*

The local cross-field plasma flux density, $\Gamma_\perp(\rho)$, must satisfy eq. (2) integrated from some point inside the separatrix, $\rho = \rho_{min}$, where $\Gamma_\perp = 0$,

$$\Gamma_\perp(\rho) = \int_{\rho_{min}}^{\rho} \left[ S_{ion} - \nabla_\parallel \Gamma_\parallel \right] \partial\rho' , \qquad (12)$$

where $S_{ion}$ is the local ionization source profile. We will be evaluating terms in eq. (12) across the profile where $Ly_\alpha$ emissivity measurements are made (see fig. 2). Here, we expect $\nabla_\parallel \Gamma_\parallel$ to be negative inside the separatrix, giving rise to a higher value of $\Gamma_\perp$ at the separatrix than that deduced from local ionization sources alone. This is the mechanism by which neutrals ionized near the X-pt appear as cross-field fluxes in the Main SOL (see fig. 7). To explore the influence of this effect, we specify a local profile of $\nabla_\parallel \Gamma_\parallel$ such that $\nabla_\parallel \Gamma_\parallel = -c_1 S_{ion}$ inside the separatrix with $c_1$ being an adjustable constant. This term leads to an additional local ion flux density through the separatrix that can be attributed to non-local ionization,

$$\Gamma_{NL}^{sep} = c_1 \int_{\rho_{min}}^{0} S_{ion} \, \partial\rho' . \qquad (13)$$

Since $S_{ion}$ is measured, this equation determines the value of $c_1$ for a specified value of $\Gamma_{NL}^{sep}$.

Outside the separatrix we expect $\nabla_\parallel \Gamma_\parallel$ to be positive. Its magnitude must be consistent with the observed flows to the divertor surfaces (e.g., fig. 7) and must balance $\Gamma_{NL}^{sep}$. To include this effect, we specify a local profile of $\nabla_\parallel \Gamma_\parallel$ outside the separatrix such that $\nabla_\parallel \Gamma_\parallel = c_2 n C_s$ where $c_2$ is another constant. The density ($n$) and sound speed ($C_s$) are evaluated locally using measurements from the horizontal scanning probe. In order to conserve particles, $c_1$ and $c_2$ must satisfy

$$c_2 \int_0^{\rho_{wall}} nC_s \partial\rho' = c_1 \int_{\rho_{min}}^{0} S_{ion} \partial\rho' . \qquad (14)$$

Note that the flux density arriving at the main chamber wall boundary is presumed to be a consequence of local ionization only,

$$\Gamma^{wall} = \int_{\rho_{min}}^{\rho_{wall}} S_{ion} \, \partial\rho' . \qquad (15)$$

We now introduce a parameter, $\alpha$, which is defined as the ratio of flux density through the separatrix due to non-local ionization divided by the flux density to the wall,

$$\alpha = \Gamma_{NL}^{sep} / \Gamma^{wall} . \qquad (16)$$

Looking at the plasma flows from the Main to the X-pt SOL regions in fig. 7, one can see that the expected range of $\alpha$ in the Main SOL is $0.23 < \alpha < 0.53$.

Finally, we arrive at a parameterized model which allows the cross-field plasma flux profile to be inferred as

$$\Gamma(\rho) = \int_{\rho_{min}}^{0} S_{ion}(1 + c_1)\partial\rho' + \int_0^{\rho} \left[ S_{ion} - c_2 \, nC_s \right] \partial\rho' , \qquad (17)$$

for $\rho \geq 0$ where $c_1$ and $c_2$ are determined from eqs. (13)-(16) and the value of $\alpha$, We now turn our attention to the measurements that will allow us to both evaluate eq. (17) and to assess the validity of the model.

*4.1.2. Ionization Source Profile Measurements*

Fig. 9 shows representative measurements of electron temperature, density, and $Ly_\alpha$ emissivity profiles for an ohmic L-mode discharge. The ionization source ($S_{ion}$) is computed from the $Ly_\alpha$ emissivity profile using the Johnson-Hinnov rate coefficients [22] and the measured plasma parameters. The derived values for $S_{ion}$ are seen to be robust; they are insensitive to the inputted values of local density and temperature. Fig. 9 shows that a simultaneous factor of 4 increase in density and temperature yields at most a factor of ~2 increase in the local value of $S_{ion}$.

*4.1.3. Wall Flux Measurements*

As outlined in section 3.1, we expect the midplane neutral pressure to be related to the flux of ions (neutrals) arriving on (leaving from) the main chamber limiter/wall surface. In the case of free molecular flow, this relationship is linear, eq. (1). Also, in a main-chamber recycling dominated regime, we expect local ionization sources to approximately balance ion fluxes on the limiter/wall. To test these assumptions, ion fluxes to the outboard limiter were measured for a series of discharges over a wide parameter range.

Fig. 10a shows the experimental arrangement: The trajectory of the horizontal scanning probe passes between two limiter structures which are separated by 0.8 meters along magnetic field lines. Owing to the short connection length, ionization can be neglected in the limiter-shadow particle balance for atomic neutral densities below ~$3 \times 10^{18}$ $m^{-3}$. (Using formalism in eq. (1), this corresponds to $P_{mid}$ ~ 1mtorr.) Thus, by integrating the ion saturation current profile across the shadow, the cross-field flux density entering the limiter-shadow ($\Gamma$ ) can be obtained.

Fig. 10b shows a comparison of $\Gamma$ and $\Gamma_W$, deduced from eq. (1), for a number of discharges spanning a wide range of parameters and core confinement regimes. For midplane pressures below ~ 0.3 mtorr ($\Gamma_W$ ~ $3.4 \times 10^{21}$ $m^{-2}$ $s^{-1}$), the estimates agree within a factor of ~2. Above ~ 0.3 mtorr there is a marked deviation, perhaps caused by the influence of neutral-neutral collisions. In any case, fig. 10(b) can be used to 'calibrate' the $P_{mid}$ measurement as a 'wall-flux meter'; $\Gamma$ can be inferred within a factor of ~2 from $P_{mid}$ using the solid black line shown in the figure.

Armed with the information from fig. 10, we can now compare the ion flux density at the radius of the outboard limiter to the ionization source computed from $Ly_\alpha$ emissivity measurements (see fig. 11). The vertical axis of fig. 11 is $\Gamma$ $(\rho_W)$ evaluated from eq. (17). The horizontal axis is

the same quantity inferred from $P_{mid}$ and the calibration curve in fig. 10. Data are shown from the same set of ohmic L-mode discharges is in fig. 3 with the addition of data from some ohmic H-modes ($1.05 < I_p < 1.35$ MA, $4 < B_T < 5.3$ tesla, $2.2\text{x}10^{20}$ m$^{-3}$ $< n_e <$ $4.2\text{x}10^{20}$ m$^{-3}$). The data support the assumption of local ionization balancing local wall fluxes; The estimates are tightly correlated and agree (to a factor of ~2), over the full range of plasma conditions. The data also lend confidence to the absolute level of the local ionization source strength inferred from $\text{Ly}_\alpha$ measurements over the full range of plasma conditions.

*4.1.4. Poloidal Flux Measurements*

Finally, we are in a position to compare the measurements of particle fluxes onto the local wall surface with particle fluxes directed towards the divertor. Fig. 12 shows particle flux directed towards the divertor (including divertor baffle) versus particle flux onto to the main chamber walls. The particle flux towards the divertor is estimated from the vertical-scanning Langmuir/Mach probe accounting for both *ExB* and parallel flows (see discussion of data in fig. 3 above). The particle flux onto the limiter/walls is estimated by multiplying the limiter ion flux density, as obtained in fig. 11, by the surface area of the main chamber plasma, ~ 7 m$^{-2}$.

Similar to the modeling results from UEDGE, these measurements indicate that the flux to the limiter/wall is larger that the flux to the divertor by a factor of ~2, implying that $\alpha$ is on the order of $\alpha \sim 0.5$. (Note that if recycling on the inner limiter is indeed higher than on the outer limiter as $\text{D}_\alpha$ measurements and recent $\text{Ly}_\alpha$ measurements suggest (see discussion in section 3.1), then $\alpha \sim 0.5$ would represent an upper bound estimate.)

*4.2. $D_{eff}$ Profiles*

We now estimate cross-field particle flux density profiles directly from measurements for a number of discharges using eq. (17). Fig. 13 shows a typical cross-field ionization density profile

($S_{ion}$) and resultant flux ($\Gamma$) for an ohmic L-mode discharge ($I_p$ = 0.8 MA, $B_T$ = 5.3 tesla, $n_e$ = 1.8x10$^{20}$ m$^{-3}$). The parameterized $\Gamma_{||}$ profiles correspond to the three values of $\alpha$ = 0, 0.5, and 1.0. Note that the value of $\Gamma$ at the separatrix correspondingly increases as $\alpha$ is increased. However, the value of $\Gamma$ at the wall is unaffected by the choice of $\alpha$, since it is fixed by the measurement. The effective particle diffusion coefficient shown in fig. 13, $D_{eff}$, is computed from the local value of $\Gamma$ divided by the local density gradient measured by the horizontal scanning probe. It should be emphasized that the use of $D_{eff}$ is not meant to imply that the transport fluxes are 'diffusive'. Rather, it is simply the diffusion coefficient that would be required to yield the observed fluxes.

$D_{eff}$ at the separatrix varies by a factor of 2 in going from $\alpha$ = 0.5 to 1. However, regardless of this variation in $\alpha$, $D_{eff}$ is see to increase by an order of magnitude in a ~10 mm distance from the separatrix. This variation is similar to that inferred by the UEDGE modeling (see fig. 5) yet the analysis technique and inputted data sets are quite different.

Applying the same analysis to 75 profiles yields the plot shown in fig. 14. Here, $\alpha$ is set to the value of 0.5 for all profiles. In all cases, $D_{eff}$ clearly increases by an order of magnitude or more within a ~10 mm distance from the separatrix. The discharges span conditions of ohmic L-mode discharges ($I_p$ = 0.8 MA, $B_T$ = 5.3 tesla, 1.0x10$^{20}$ m$^{-3}$ < $n_e$ < 2.3x10$^{20}$ m$^{-3}$) and EDA or Elm-free H-mode discharges (1.0 < $I_p$ < 1.4 MA, 4.0 < $B_T$ < 5.6 tesla, 2.2 < $n_e$ < 4x10$^{20}$ m$^{-3}$).

H-mode discharges have the lowest $D_{eff}$ at the separatrix, causing the strongest variation in $D_{eff}$ across the SOL. The values of $D_{eff}$ in the far SOL appear to be roughly similar in the L- and H-mode regimes.

Perhaps the most interesting observation that can be gleaned from fig. 14 is the following: Even allowing for the sensitivity to the model assumptions, a factor of ~10 variation in the value of $D_{eff}$ at a fixed spatial location should be well outside the error bars. This suggests that most of the discharge-to-discharge variation in the inferred $D_{eff}$ profiles is caused by a change in the transport level. Note that the UEDGE modeling of two discharges (fig. 5) required a substantial increase in $D_{eff}$ across the whole profile in going from the low- to high-$P_{mid}$ discharge. Now using this direct experimental technique, $D_{eff}$ profiles can be studied in many discharges, allowing trends in the scaling of $D_{eff}$ with local or global conditions to be inferred.

*4.3. $D_{eff}$ Scalings*

At the present time, the $D_{eff}$ profiles shown in fig. 14 represent the full extent of our data. Focussing on the ohmic L-mode portion of the data set, the first step is to look for correlations between the local value of $D_{eff}$ and the local value of electron temperature ($T_e$) and density ($n$). It should be noted that since these measurements are at fixed plasma current and toroidal field, correlations with $I_p$ and $B_T$ (or dimensionless equivalents) can not yet be performed.

Fig. 15 shows the result of a regression analysis between $D_{eff}$ and the local values of $T_e$ and $n$ at the $\rho$ = 2 mm location. The order-of-magnitude variation of $D_{eff}$ seen in fig. 14 at this flux surface location does indeed collapse into a reasonable correlation with the local values of $T_e$ (eV) and $n$ ($m^{-3}$),

$$D_{eff} \sim 0.069\ (T_e/50)^{-3.5}\ (n/10^{20})^{1.7} \qquad (m^2\ s^{-1}). \qquad (18)$$

For comparison, the values of $D_{eff}$ at $\rho$ =2 mm from the two UEDGE simulations described above (fig. 5) are also plotted in fig. 15 (square symbols). These two 'data points' were not used in the regression. The horizontal axis for the UEDGE points is evaluated using the measured local values

of $T_e$ and $n$ at the $\rho$ = 2 mm. The UEDGE and local particle balance-derived $D_{eff}$ values scale very similarly. The agreement of the absolute levels of $D_{eff}$ is also reasonable. In the UEDGE case, $D_{eff}$ represents the flux-surface averaged value while the local particle balance model does not account for magnetic flux surface compression, using the local density gradient at the midplane.

The scaling relationship implied by fig. 15 is an interesting one that suggests a rather simple correlation between $D_{eff}$ near the separatrix and the collisionality of the plasma: $D_{eff} \sim \lambda_{ei}^{-1.7}$, where $\lambda_{ei}$ is the electron-ion mean-free path. Performing similar regression analyses on $D_{eff}$ at different spatial locations in the SOL (see table I) leads to similar trends in a ~5 mm region near the separatrix. Further out in the SOL, the scaling relationship changes, favoring a weaker correlation, if any, of $D_{eff}$ with local $T_e$.

In addition to the fitted parameters, table I shows the results of performing partial *F*-test evaluation of the regressors, $T_e$ and $n$ (columns labeled '$T_e$ *F*-test' and '$n$ *F*-test', respectively). The square of the multiple correlation coefficient ($R^2$) for each fit is also shown [33]. When the partial *F*-test value is greater than 12.0 (for the ~60 data points), then there is less than a 0.1% chance of obtaining the same degree of correlation with random values substituted for that regressor. Thus for *F*-test values less than ~12.0, we may conservatively consider that the regressor may be either 'uncorrelated' with $D_{eff}$ or 'redundant' with another regressor or that the data is 'too noisy' to extract a meaningful correlation. With the possible exception of the data at $\rho$ = 14 mm, reasonable correlations of $D_{eff}$ with the local values of $T_e$ and/or $n$ are clearly detected.

One should be aware that in addition to 'noise' there may be systematic trends built into the computation of $D_{eff}$ which have not been taken into account at this time. For example the parameter, $\alpha$, used to evaluate eq. (17) is likely to be a function of plasma conditions. Looking at the UEDGE results, we see that there is a trend for $\alpha$ to get smaller (.53 $\rightarrow$ .23) as the plasma

density (or $P_{mid}$) gets larger. However, the good agreement between the UEDGE and local particle balance derived values of $D_{eff}$ seen in fig. 15 lends some confidence that corrections of this type are minor.

*4.4. Cross-field Heat Convection → Density Limit?*

From the scalings of $D_{eff}$ derived above, one expects that cross-field heat convection near the separatrix should play an increasing role in the SOL power balance as the collisionality increases. Fig. 16 shows $D_{eff}$ inferred at $\rho$ = 1 mm and the corresponding fraction of the SOL power convected by electrons and ions at this location,

$$f_{conv} = 5 T_e \Gamma \; A_{sep} / P_{sol}, \tag{19}$$

where $P_{sol}$ is the power crossing the separatrix, $A_{sep}$ is the area of the separatrix, and it is assumed that $T_i \approx T_e$. The data are plotted versus $\lambda_{ei} / L$ which is the electron-ion mean free path normalized to 1/2 the parallel magnetic connection length. These data are from the same set of discharges shown in fig. 14.

As the regression analysis suggested, fig. 16 shows that the discharge-to-discharge variation in $D_{eff}$ is well correlated with the variation in local collisionality, $\lambda_{ei} / L$. Although there is not enough data from H-mode discharges to investigate a correlation of $D_{eff}$ with local collisionality, it is clear from fig. 16 that $D_{eff}$ near the separatrix is greatly reduced in H-mode discharges with the same local collisionality. The range of core densities in these discharges was $0.1 < n / n_G < 0.35$, where $n_G$ is the Greenwald density [34]. The collisionality of the SOL is found to increase monotonically with increasing $n / n_G$. Correspondingly, the convected power into the SOL increases, rising to a maximum level in these discharges of $f_{conv} \sim 0.2$.

Although the behavior of the SOL particle transport has not yet been studied with this technique for core densities approaching the Greenwald density limit, these initial results are very interesting. The UEDGE modeling in section 3.3.2 clearly showed that electron heat convection and charge exchange losses through the separatrix become more important as the particle flux through the SOL is increases. The empirical scaling identified above of cross-field particle transport near the separatrix increasing with collisionality naturally leads to a situation at high plasma densities where cross-field convection and charge exchange carry most of the power across the separatrix. In this case, there would exist a critical plasma density (~ collisionality) beyond which no steady-state plasma could be maintained. In contrast to a density limit set by radiative collapse, this density limit would be fundamentally set by the physics of anomalous transport processes since it would exist even in the absence of radiation.

**5. Summary**

Contrary to the ideal picture of divertor operation, the divertor in Alcator C-Mod receives only part of the total particle efflux from the main-chamber plasma. The reason for this discrepancy is not caused by the tight divertor baffling but rather the existence of cross-field particle transport in the main-chamber scrape-off layer (MCSOL) that is large and increases with distance into the SOL, carrying plasma to main-chamber limiter/wall surfaces.

This ‘main-chamber recycling’ regime, where ionization in the SOL is primarily balanced by cross-field particle fluxes, can be understood with the aid of a simplified plasma/neutral particle balance model: When the flux-surface averaged neutral density exceeds a critical value, flows to the divertor can no longer compete with the ionization source and particle fluxes must increase with distance into the SOL. This critical neutral density condition can be recast into a critical cross-field plasma flux condition: particle fluxes must increase with distance into the SOL when the plasma

flux crossing a given flux surface exceeds a critical value. Thus, the existence of the 'main-chamber recycling' regime is intrinsically tied to the level of anomalous cross-field particle transport.

Density profiles in the SOL are always seen to decay ~exponentially with distance from the separatrix. In the past, this observation lead to the naïve interpretation that plasma flow to the divertor (or baffle plate) was dominating the SOL particle balance and that the effective particle diffusion coefficient ($D_{eff}$) was ~constant in space. This interpretation was clearly wrong. Within this context of a diffusive plasma transport model, one must conclude that $D_{eff}$ increases rapidly with distance from the separatrix in order to account for the 'exponential' density profiles in the absence of strong parallel flows to the divertor/baffle structures.

As a consequence of large cross-field particle transport, cross-field heat convection and charge exchange play a significant role the power balance of the C-Mod SOL, particularly in the far SOL. Except near the separatrix in low density discharges, heat flux arising from anomalous cross-field heat diffusivity ($\chi_\perp$) is a minor contributor, making extraction of this parameter from profile data difficult.

Using Langmuir/Mach probes and VUV diodes, the fluxes to main-chamber wall surfaces, fluxes into the divertor, and ionization profiles across the main-chamber scrape-off layer have been directly monitored. These measurements have allowed $D_{eff}$ profiles to be inferred systematically in a number of discharges. Regression analysis of a small set of ohmic L-mode data indicates that $D_{eff}$ near the separatrix is strongly correlated with the local values of density and temperature suggesting a direct correlation with plasma collisionality: $D_{eff} \sim \lambda_{ei}^{-1.7}$, where $\lambda_{ei}$ is the electron-ion mean-free path.

Although this relationship between particle transport and collisionality (or ~equivalently, discharge density) needs to be born out with more data, is an interesting one. It is pointed out that

this relationship would naturally lead to a plasma density beyond which no steady-state plasma could be maintained, even in the absence of radiation.

**Acknowledgements**

These results were made possible by the excellent engineers, technical staff, students, and scientists on the Alcator team. Discussions of recycling behavior on JT-60U with Dr. Asakura are gratefully acknowledged. This work is supported by U.S. D.o.E. Coop. Agreement DE-FC02-99ER54512.

## References


[1] Umansky, M.V., Krasheninnikov, S.I., LaBombard, B., and Terry, J.L., Phys. Plasmas **5** (1998) 3373.

[2] LaBombard, B., et al., J. Nucl. Mater. **241-243** (1997) 149.

[3] McCormick, K., et al., in Controlled Fusion and Plasma Physics (Proc. 20th Eur. Conf., Lissabon, 1993), Vol. 2, European Physical Society, Geneva (1993) 597.

[4] Asakura, N., et al., J. Nucl. Mater. **241-243** (1997) 559.

[5] Bosch, H.S., et al., J. Nucl. Mater. **220-220** (1995) 558.

[6] Asakura, N., et al., J. Nucl. Mater. **266-269** (1999) 182.

[7] Pitcher, C.S., et al., Phys. Plasmas **7** (2000) 1894.

[8] Pitcher, C.S., et al., submitted to J. Nucl. Mater.

[9] Bosch, H.S., et al., J. Nucl. Mater. **266-269** (1999) 462.

[10] Schneider, R., et al., J. Nucl. Mater. **266-269** (1999) 175.

[11] Allen, S.L., et al., J. Nucl. Mater. **266-269** (1999) 168.

[12] Vlases, G.C., et al., J. Nucl. Mater. **266-269** (1999) 160.

[13] Umansky, M.V., Krasheninnikov, S.I., and LaBombard, B., Phys. Plasmas **6** (1999) 2791.

[14] Rognlien, T.D., Milovich, J.L., Rensink, M.E., and Porter, G.D., J. Nucl. Mater. **196-198** (1992) 347.

[15] Hutchinson, I.H., et al., Phys. Plasmas **1** (1994) 1511.

[16] Boivin, R.L., et al., Phys. Plasmas **7** (2000) 1919.

[17] Post, D.E., J. Nucl. Mater. **220-222** (1995) 143.

[18] Mossessian, D. and Hughes, J., to be published in Rev. Sci. Instrum.

[19] Hutchinson, I.H., Phys. Fluids **30** (1987) 3777.

[20] Granetz, R.S., Hutchinson, I.H., Gerolamo, J., Pina, W., and Tsui, C., Rev. Sci. Instrum. **61** (1990) 2967.

[21] Lao, L.L., et al., Nucl. Fusion **25** (1985) 1611.

[22] Johnson, L.C. and Hinnov, E., J. Quant. Spectrosc. Radiat. Transfer **13** (1973) 333.

[23] Boivin, R.L. et al., to be published in Rev. Sci. Instrum.

[24] Owen, L., et al., Bull. Amer. Phys. Soc. **43** (1998) 1823.

[25] Mioduszewski, P., et al., Bull. Amer. Phys. Soc. **44** (1999) 208.

[26] Nachtrieb, R.T. and LaBombard, B., to be published in Phys. Plasmas.

[27] Shimizu, K., Itami, K., Kubo, H., Asakura, N., and Shimada, M., J. Nucl. Mater. **196-198** (1992) 476.

[28] Erents, S.K., et al., J. Nucl. Mater. **241-243** (1997) 433.
[29] Erents, S.K. and Stangeby, P.C., Nucl. Fusion **38** (1998) 1637.
[30] LaBombard, B., et al., in Plasma Physics and Controlled Fusion Research 1996 (Proc. 14th Int. Conf., Montreal, 1996), Vol. 1, IAEA, Vienna (1997) 825.
[31] Connor, J.W., et al., Nucl. Fusion **39** (1999) 169.
[32] Counsell, G.F., et al., J. Nucl. Mater. **266-269** (1999) 91.
[33] Bevington, P.R., *Data reduction and error analysis for the physical sciences* (McGraw-Hill, New York, 1969).
[34] Greenwald, M., et al., Nucl. Fusion **28** (1988) 2199.

*Table I –Regression analysis: Correlation of $D_{eff}$ measured at various spatial locations with local $T_e$ and n during an ohmic L-mode density scan*

| Location $\rho$ (mm) | $D_{eff}^*$ ($m^2\ s^{-1}$) | $\alpha$ | $\beta$ | Te F-test | n F-test | $R^2$ |
|---|---|---|---|---|---|---|
| 1 | 0.07 | -3.7 | 2.2 | 97.3 | 126.9 | 0.74 |
| 2 | 0.07 | -3.5 | 1.7 | 121.5 | 112.1 | 0.73 |
| 3 | 0.07 | -3.2 | 1.2 | 90.8 | 56.0 | 0.64 |
| 4.5 | 0.09 | -3.1 | 1.2 | 76.5 | 64.0 | 0.63 |
| 6.5 | 0.31 | -2.1 | 1.4 | 40.4 | 139.4 | 0.72 |
| 10 | 1.03 | -0.6 | 1.0 | 2.8 | 78.5 | 0.71 |
| 14 | 0.64 | -0.7 | 0.5 | 5.1 | 18.0 | 0.30 |

$$D_{eff} = D_{eff}^* \, (T_e/50\ eV)^{\alpha} \, (n/10^{20}\ m^{-3})^{\beta}$$

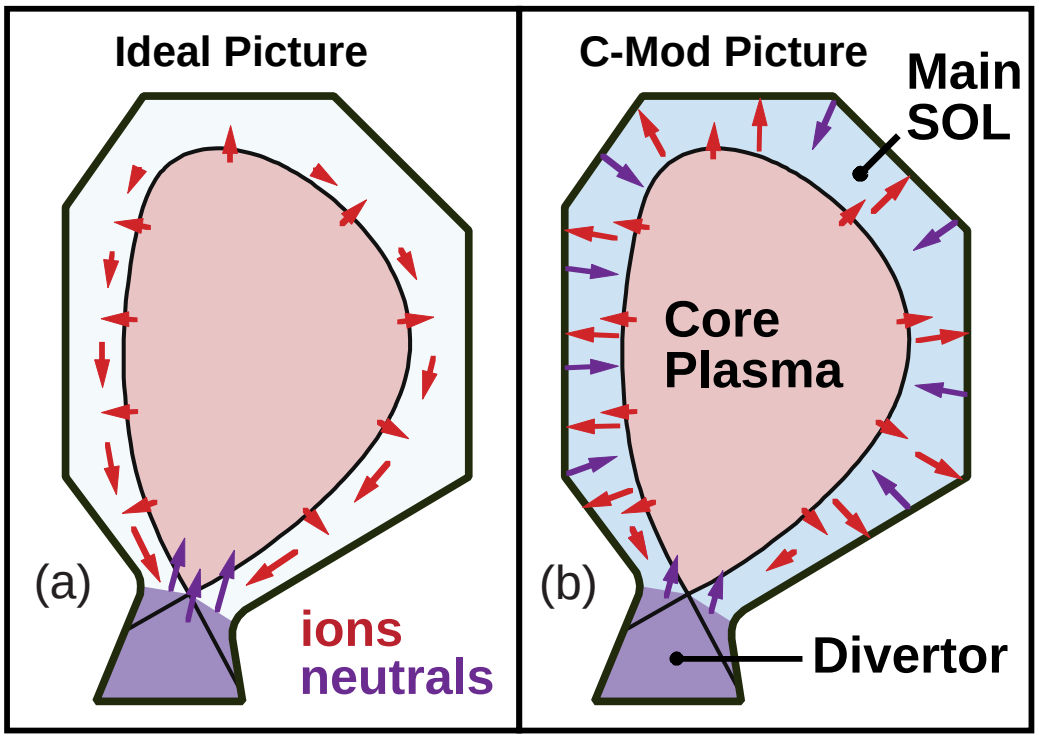


*Fig. 1. In ideal divertor operation (a), all plasma crossing the separatrix neutralizes in the divertor. X-point ionization fuels the core. Diverted plasmas in Alcator C-Mod do not behave in this way (b). This is owing to rapid transport in the far scrape-off layer (SOL), carrying plasma to the main-chamber walls.*

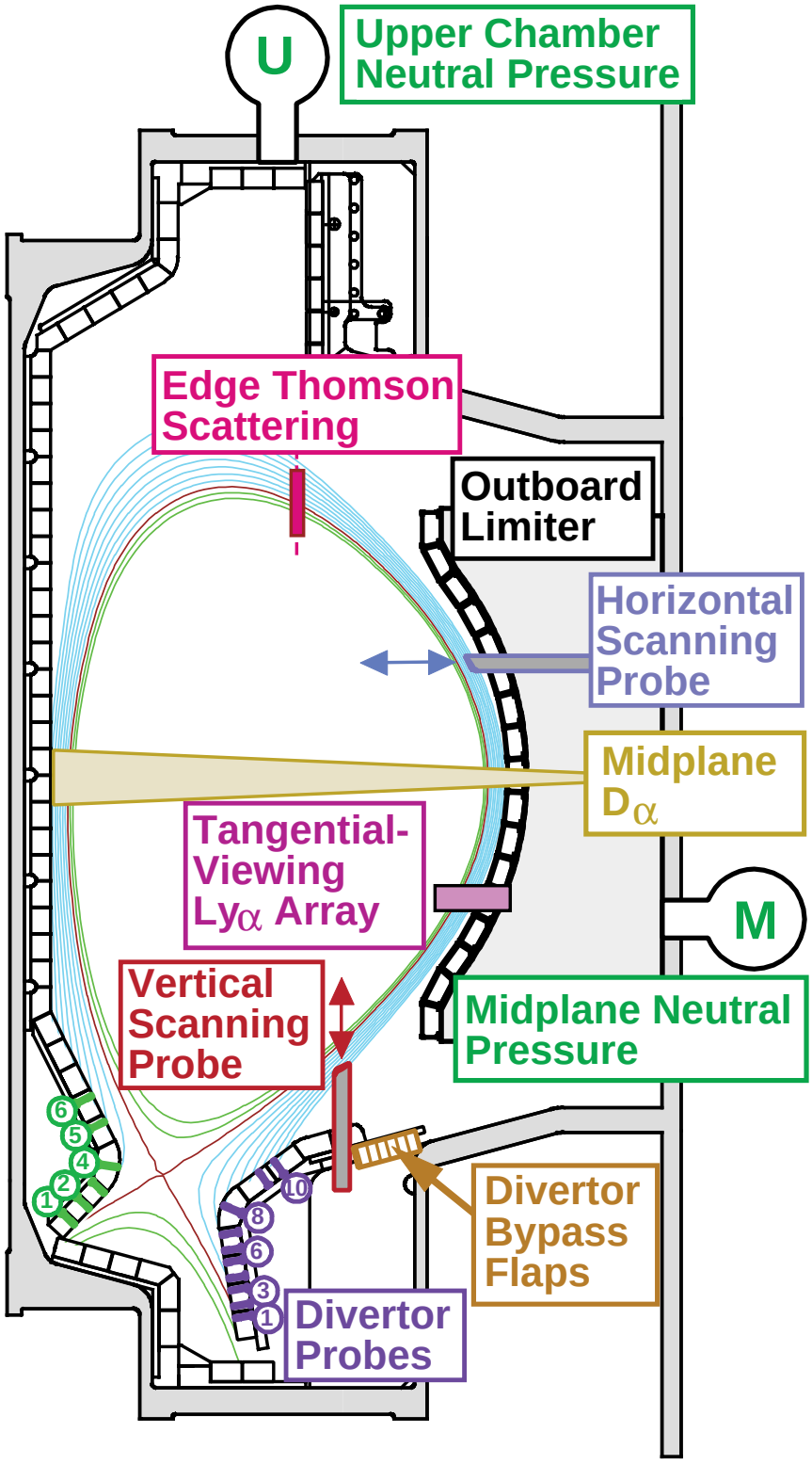


*Fig. 2. Cross-section of Alcator C-Mod showing divertor geometry, edge plasma diagnostics and a typical plasma equilibrium used for these studies. Each magnetic flux contour corresponds to a* $\Delta\rho = 2$ *mm radial separation at the midplane. In this paper, the separatrix is designated as* $\rho = 0$ *and the scrape-off layer as* $\rho > 0$.

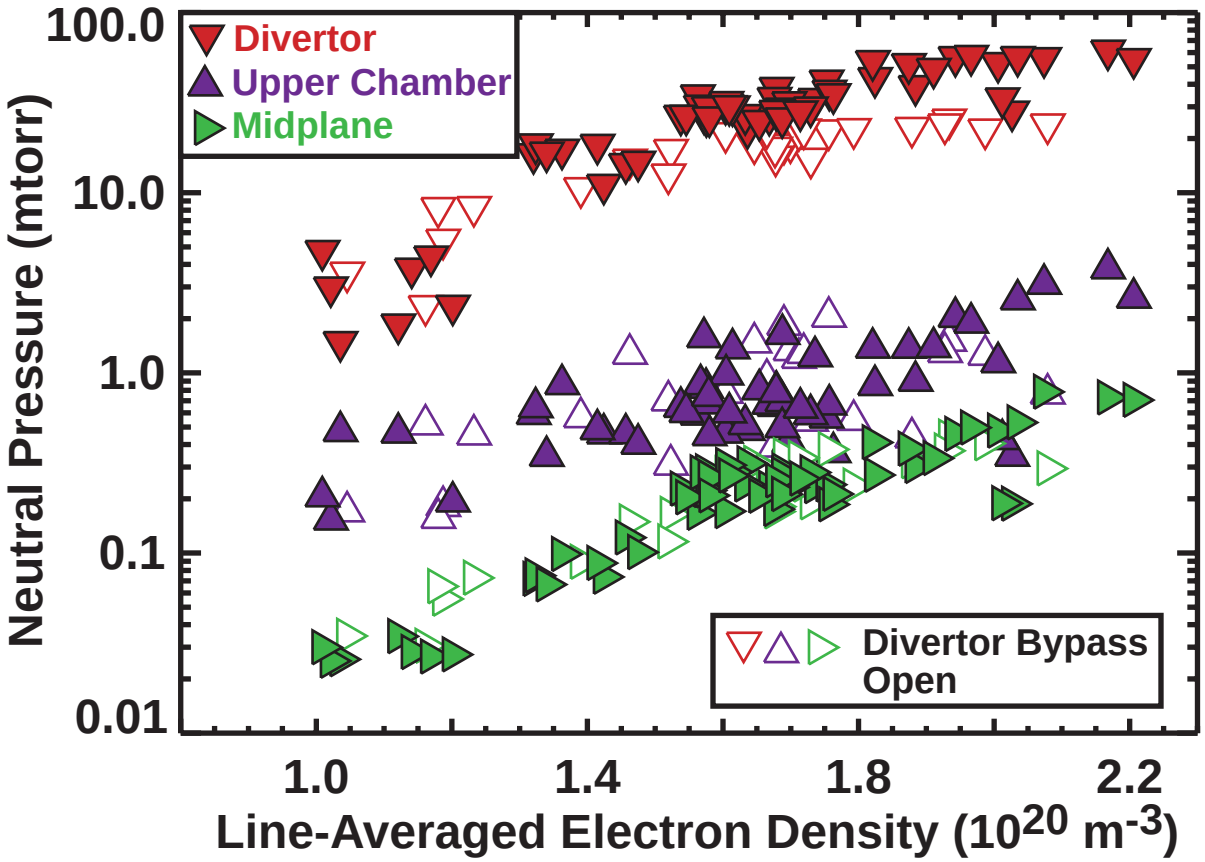


*Fig. 3. Neutral pressures in divertor, upper chamber, and midplane locations as a function of line-average electron density during an ohmic L-mode density scan. Open symbols refer to measurements taken with the divertor bypass valve [7,8] open.*

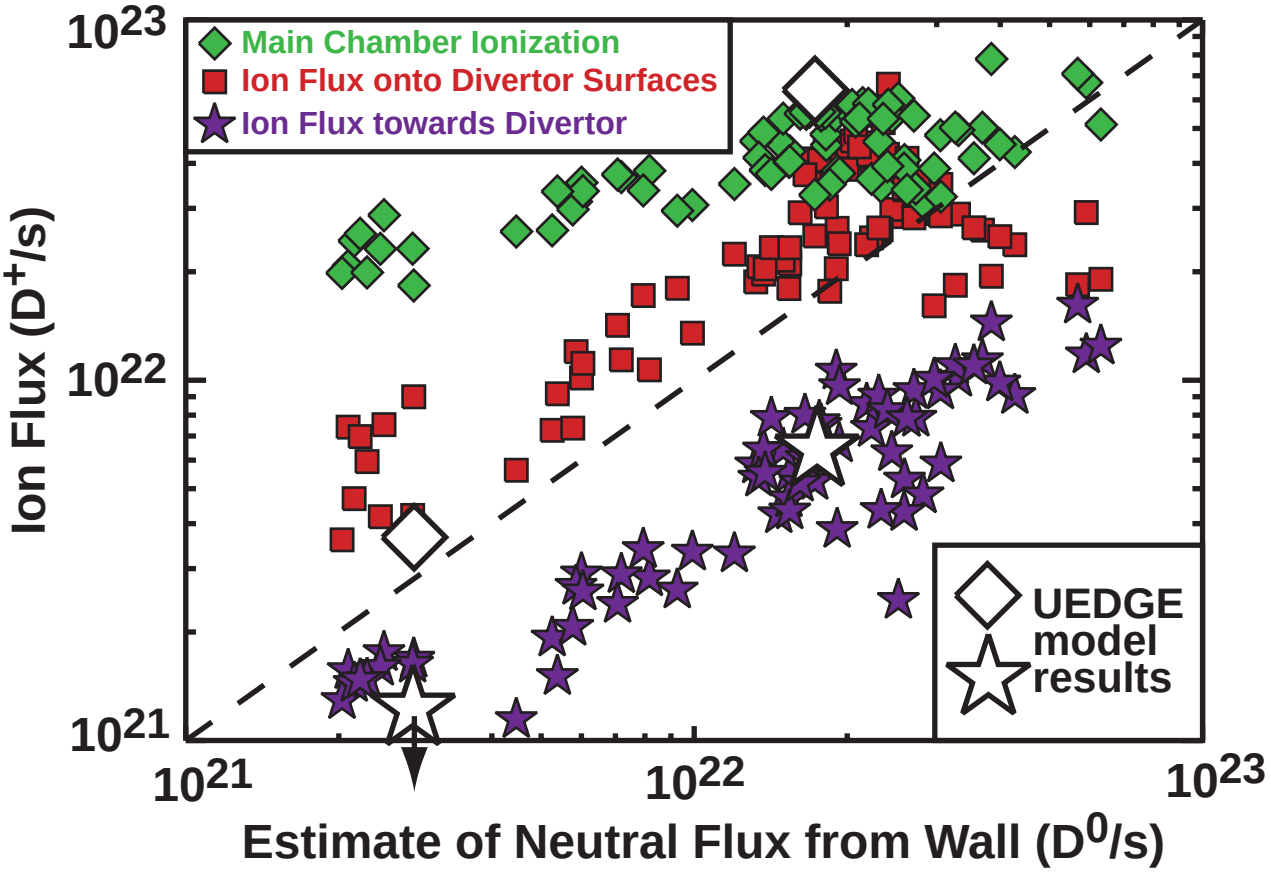


*Fig. 4. Rough estimates of ionization fluxes in the main chamber from midplane $D_\alpha$ (◆), ion fluxes towards the divertor from scanning Langmuir/Mach probe (★), and ion fluxes onto divertor surfaces from divertor probes (■) as a function of an estimate of neutral flux from the wall using eq. (1). UEDGE simulation of two discharges yields similar result: fluxes from main chamber ionization (◊) are much higher than fluxes directed toward the divertor (☆).*

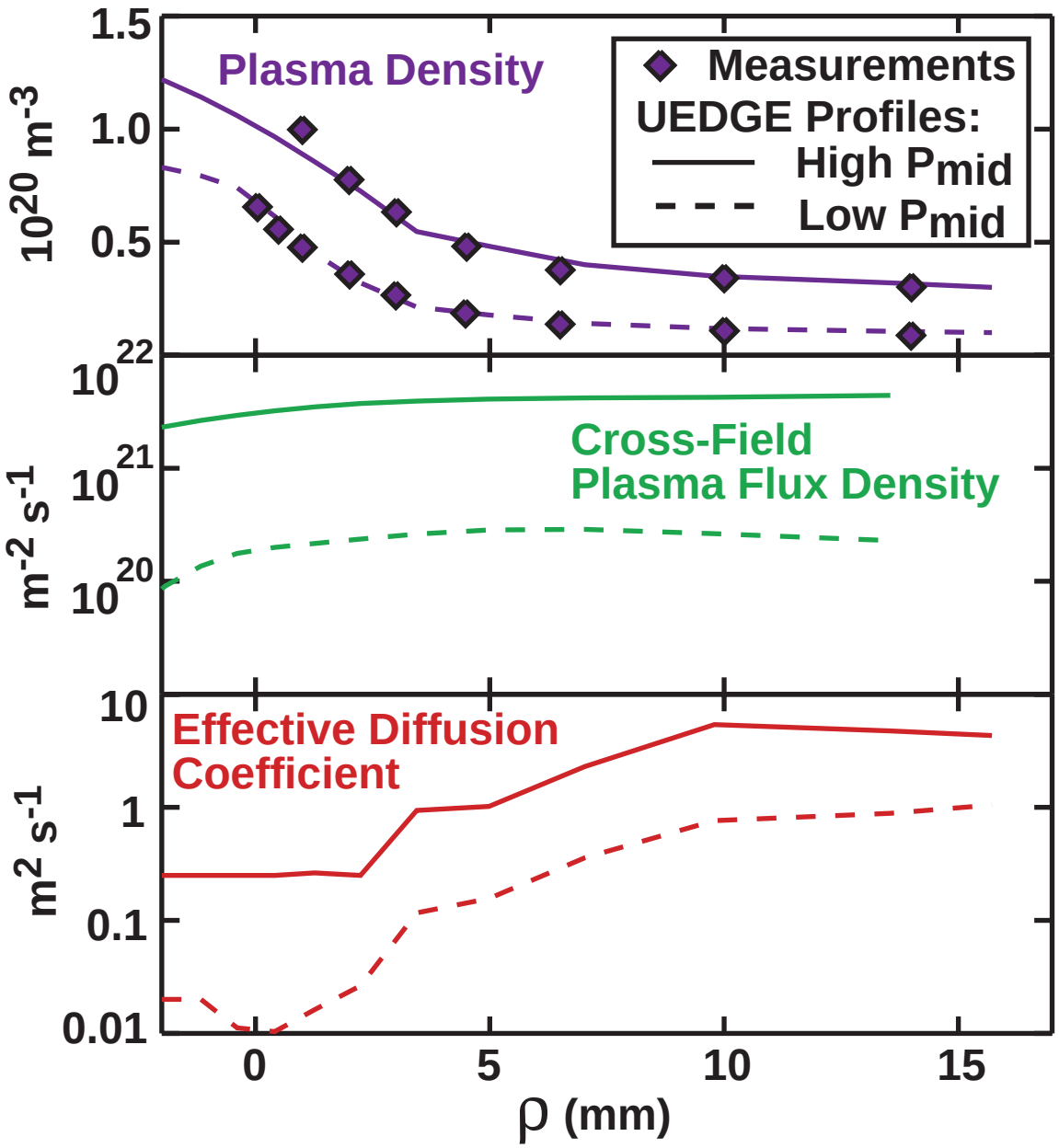


*Fig. 5. Results from UEDGE modeling of two ohmic L-mode discharges with high (0.3 mtorr) and low (.025 mtorr) midplane pressure [12]. In both cases the cross-field particle flux density is ~ constant or increasing with* ρ. *This requires that* $D_{eff}$ *increase sharply with* ρ.

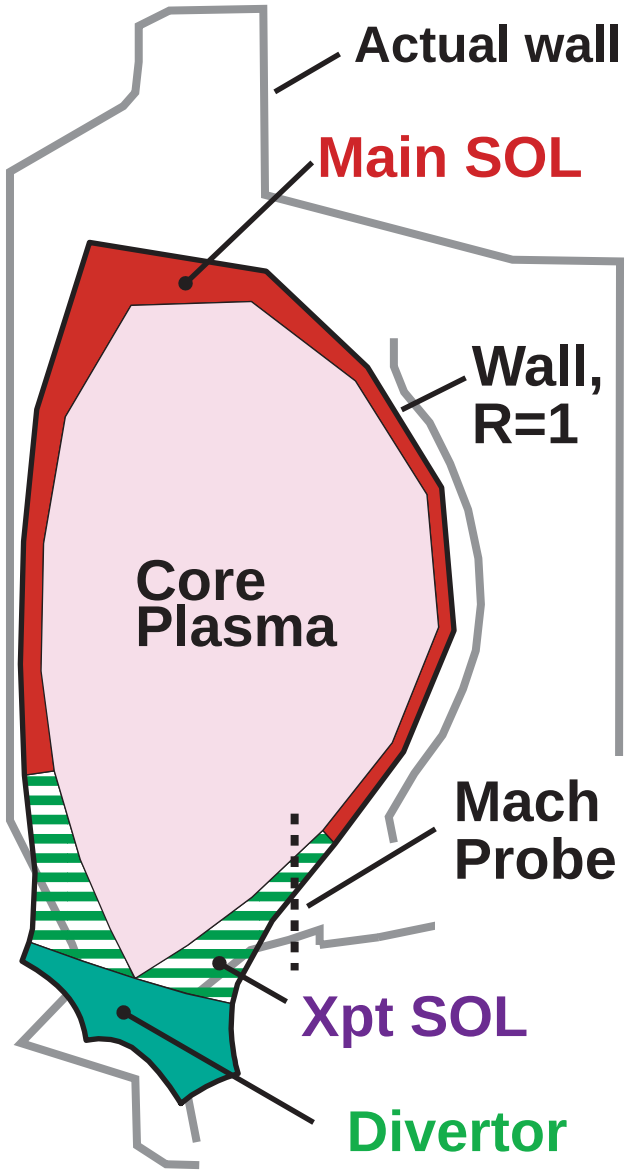


*Fig. 6. Particle balance in the UEDGE simulations can be tracked via ion/neutral exchange between 4 plasma regions: Core Plasma, Main SOL, X-pt SOL, and Divertor. Ion flow between Main SOL and X-pt SOL regions simulates fluxes measured by the vertical-scanning Langmuir/Mach probe.*

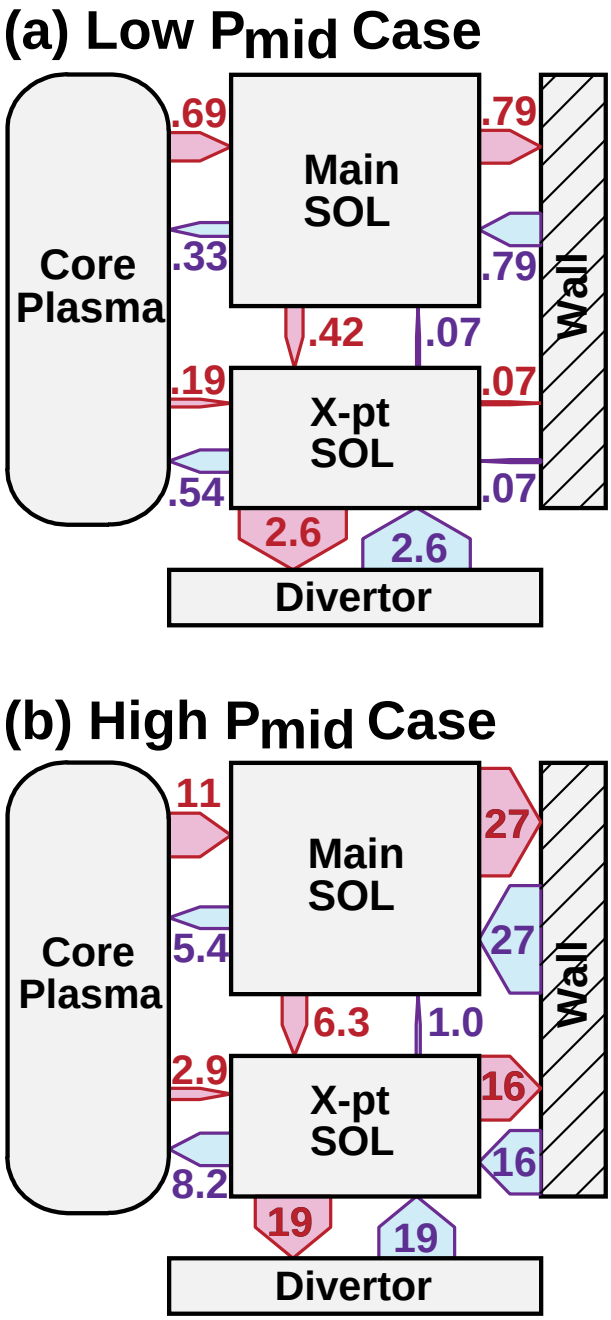


*Fig. 7. Ion (pink) and neutral (blue) fluxes (units of $10^{21}$ $s^{-1}$) communicating between plasma regions in UEDGE simulations of (a) low $P_{mid}$ and (b) high $P_{mid}$ cases. In both cases, the ion flux from Main SOL → Wall is larger than Main SOL → X-pt SOL.*

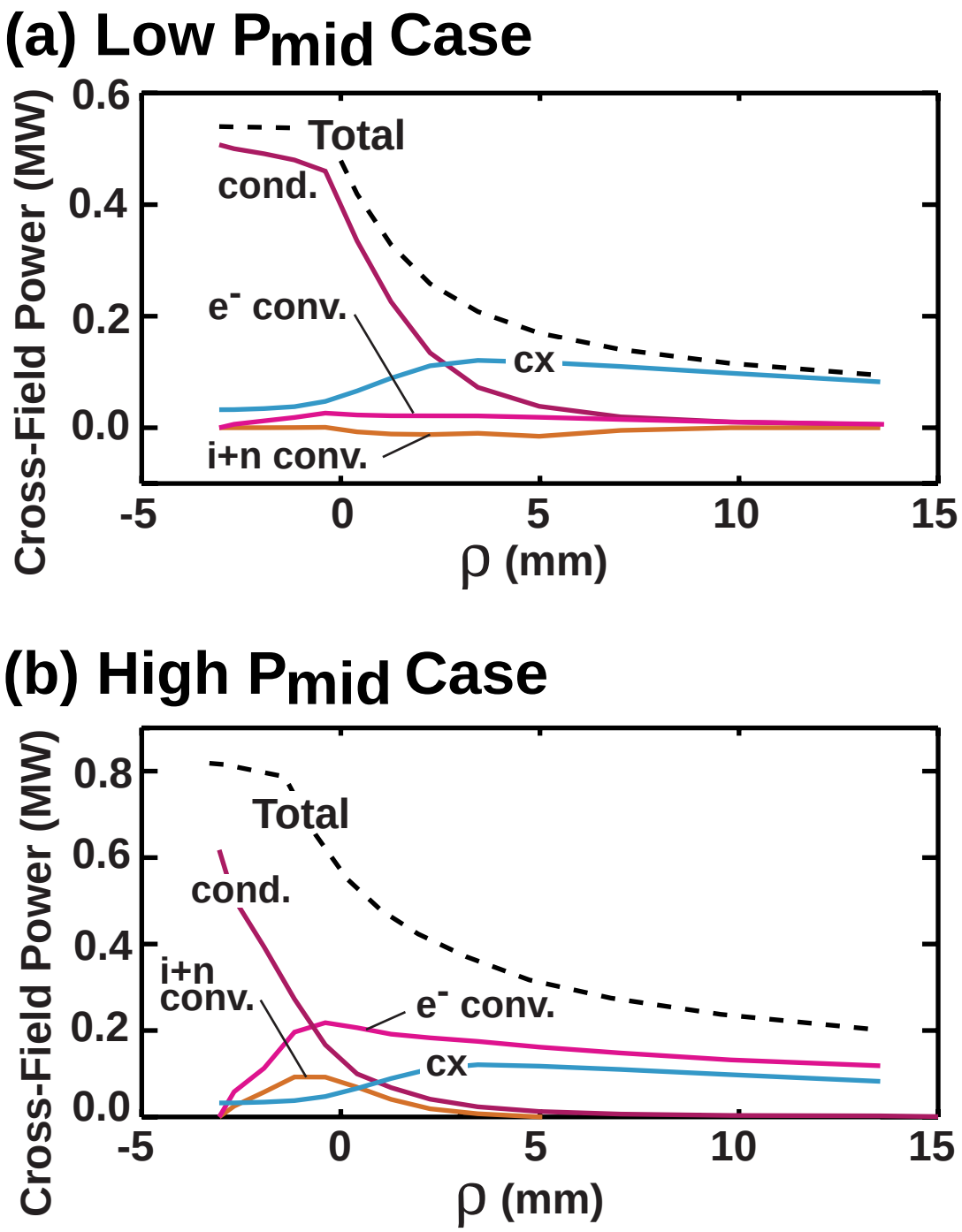


*Fig. 8. Contributions to the cross field power flux profiles in (a) low $P_{mid}$ and (b) high $P_{mid}$ discharges simulated by UEDGE. Charge exchange (CX) and electron convection ($e^-$ conv.) dominate the heat transport in the far SOL. At high $P_{mid}$, electron convection dominates the whole SOL. Cross-field heat conduction plays a role only near the separatrix in the low $P_{mid}$ case.*

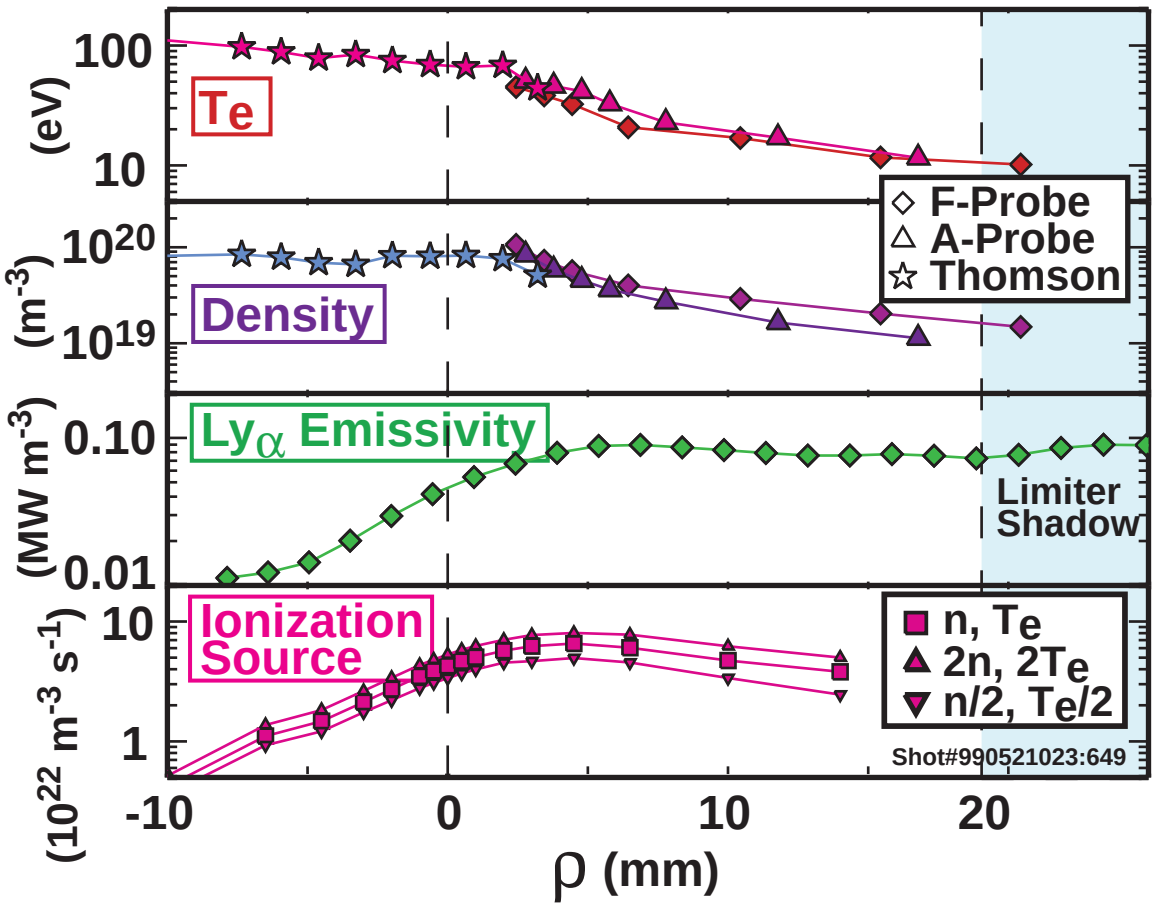


*Fig. 9. Cross-field profiles electron temperature, density, and $Ly_\alpha$ emissivity profiles from a representative discharge (top three panels). The ionization source profile (last panel) is derived using Johnson-Hinnov rate coefficients [22]. The sensitivity of the ionization profile to a factor of 2 and 1/2 multiplier on the electron temperature and density measurements is shown.*

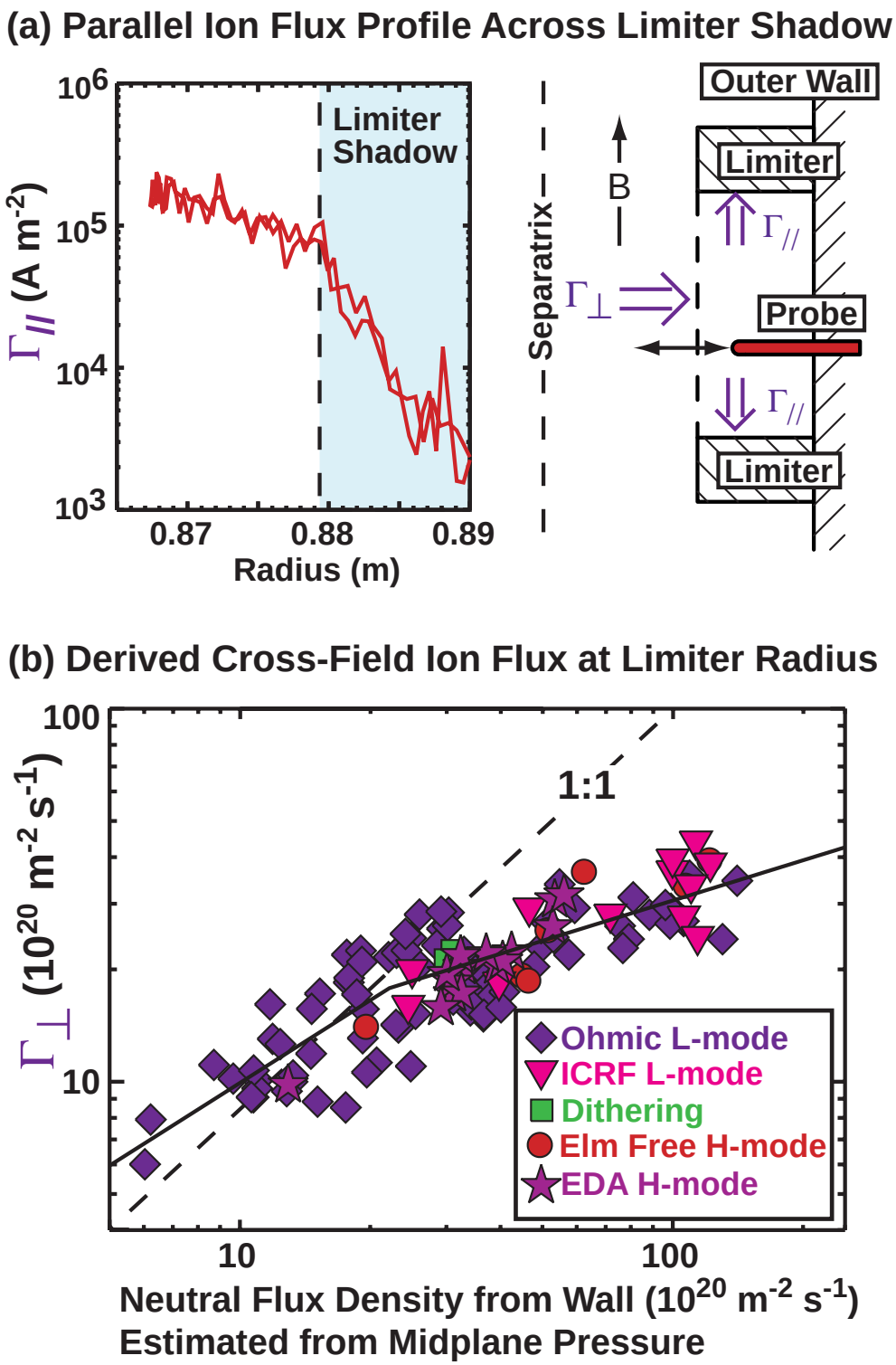


*Fig. 10. (a) Measurement of the parallel ion flux profile, $\Gamma_{||}$, in the shadow of a main-chamber limiter is used to infer the cross-field particle flux at the limiter radius, $\Gamma_{\perp}$. (b) $\Gamma_{\perp}$ in a number of discharges is compared to the neutral flux estimated from eq. (1) and the midplane neutral pressure. A calibration curve (solid line) allows $\Gamma_{\perp}$ to be estimated directly from midplane neutral pressure.*

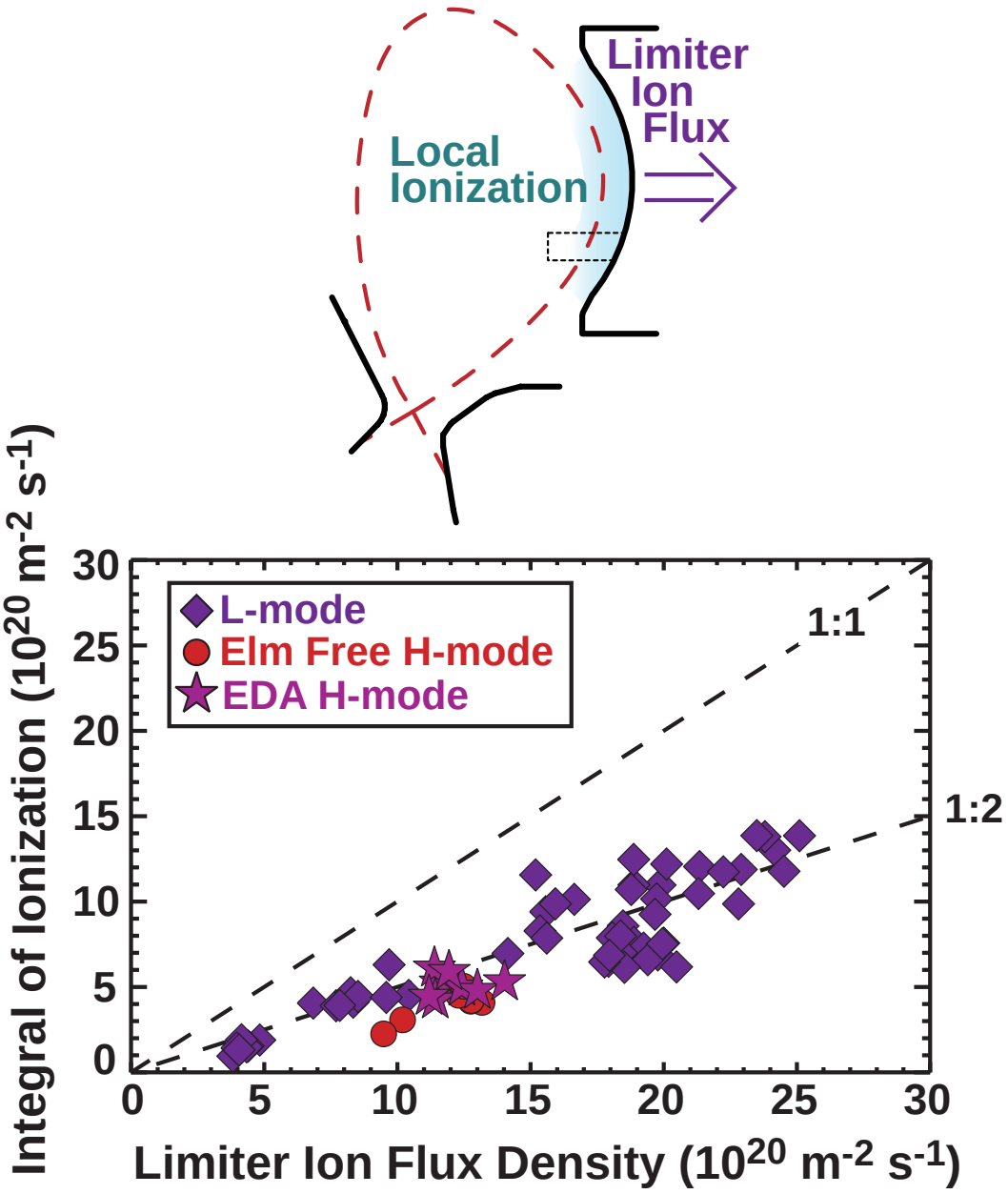


*Fig. 11. Comparison of cross-field ion flux density at the limiter radius. Vertical axis is $\Gamma_\perp$ derived from integrating the ionization profile (inferred from $Ly_\alpha$ emissivity profiles). Horizontal axis is $\Gamma_\perp$ derived from limiter particle flux estimates using the midplane pressure and the calibration curve in fig. 10.*

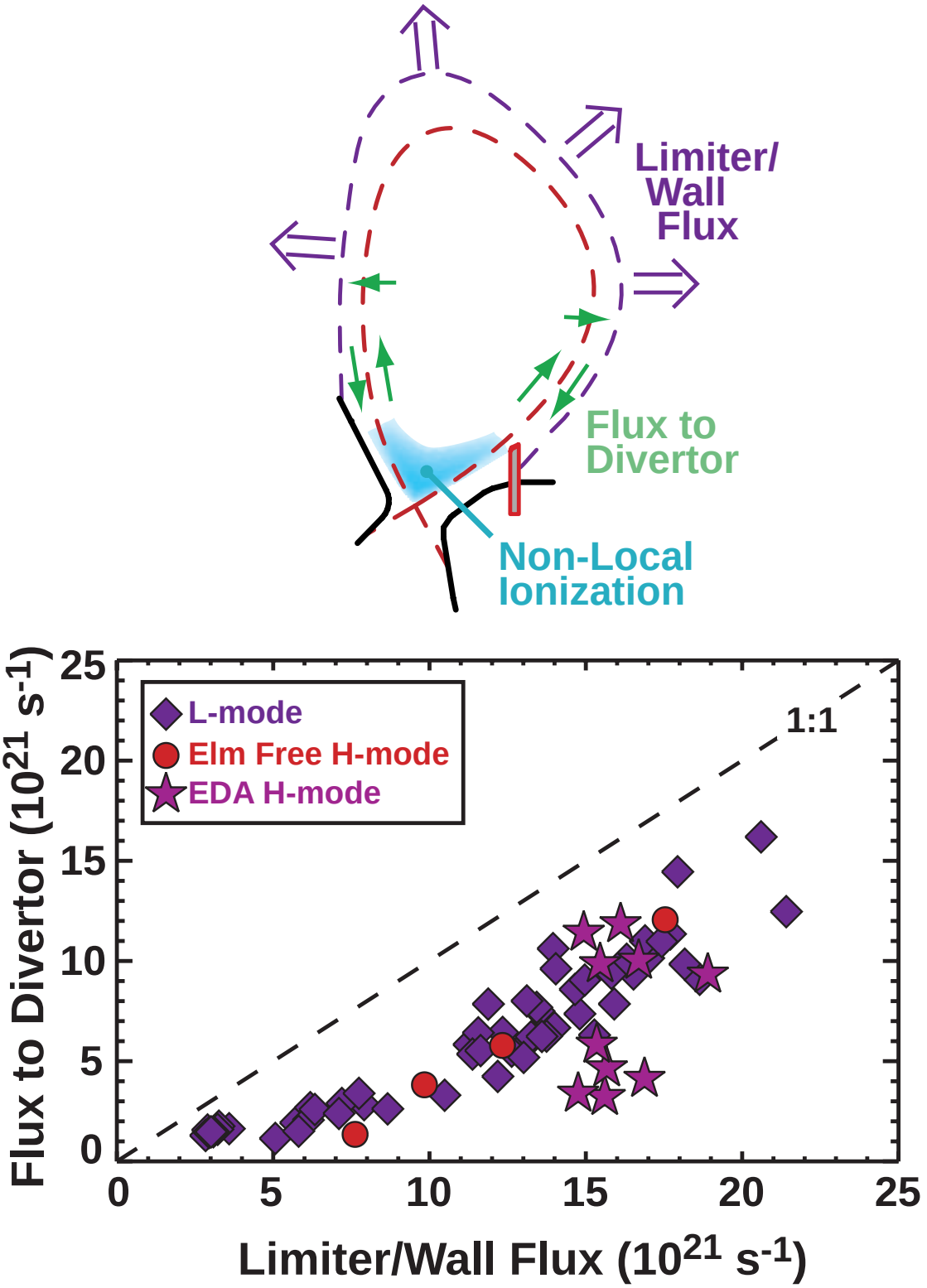


*Fig. 12. Particle flux directed towards divertor (estimated from Langmuir/Mach probe measurements) versus particle flux onto main-chamber wall surface (estimated from midplane limiter fluxes). Flux toward divertor is ~1/2 the level of flux arriving on the main-chamber limiter/wall.*

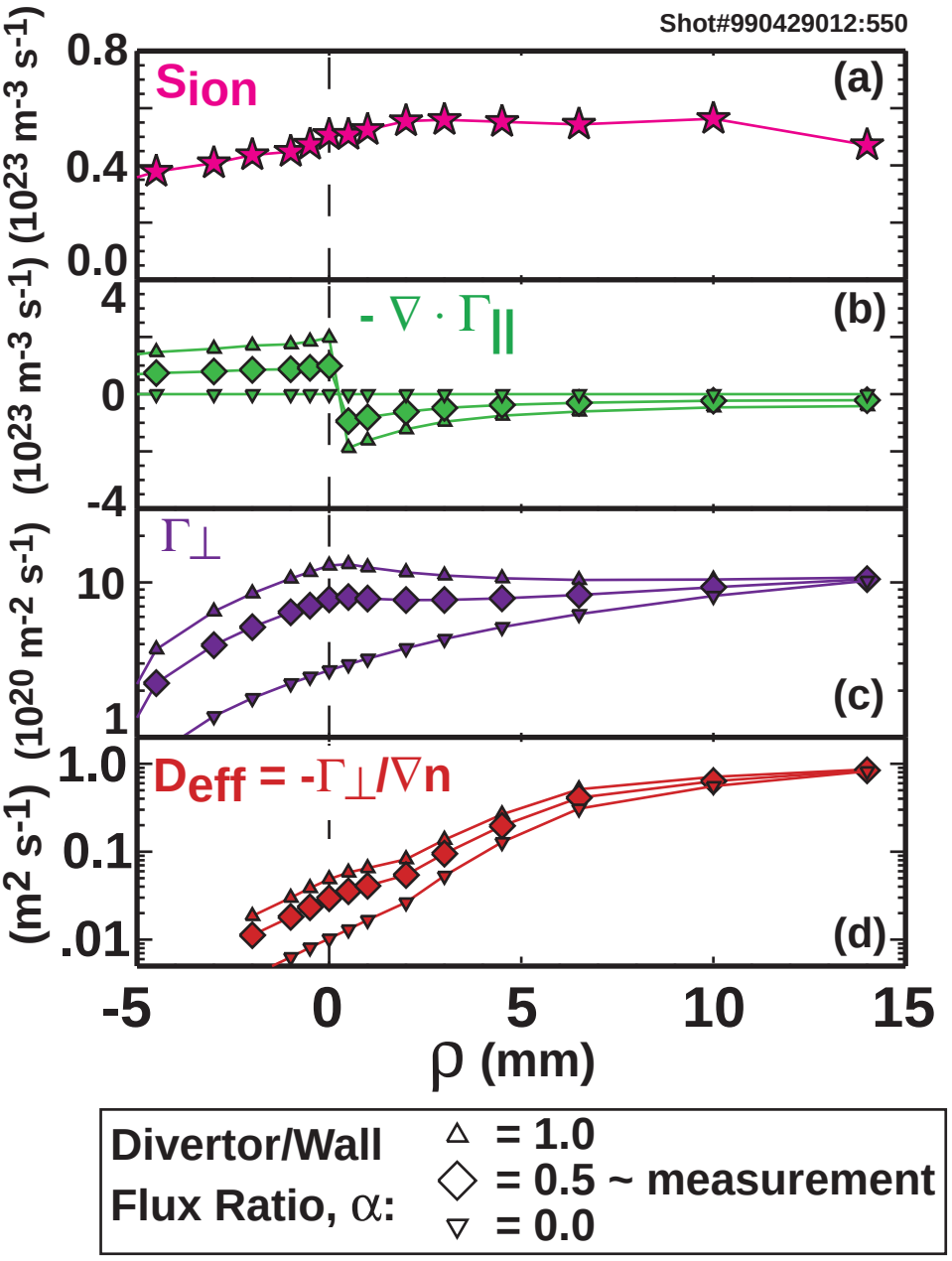


*Fig. 13. (a) Ionization source profile (measured), (b) divergence of parallel flow profiles (modeled), (c) resultant cross-field particle flux density profiles and (d) effective particle diffusivity profiles from eq. (17). The magnitude of* $\nabla_{\|} \cdot \Gamma_{\|}$ *and resultant* $\Gamma_{\perp}$ *and* $D_{eff}$ *profiles depend on the ratio of particle fluxes to divertor/wall (≡* $\alpha$*).*

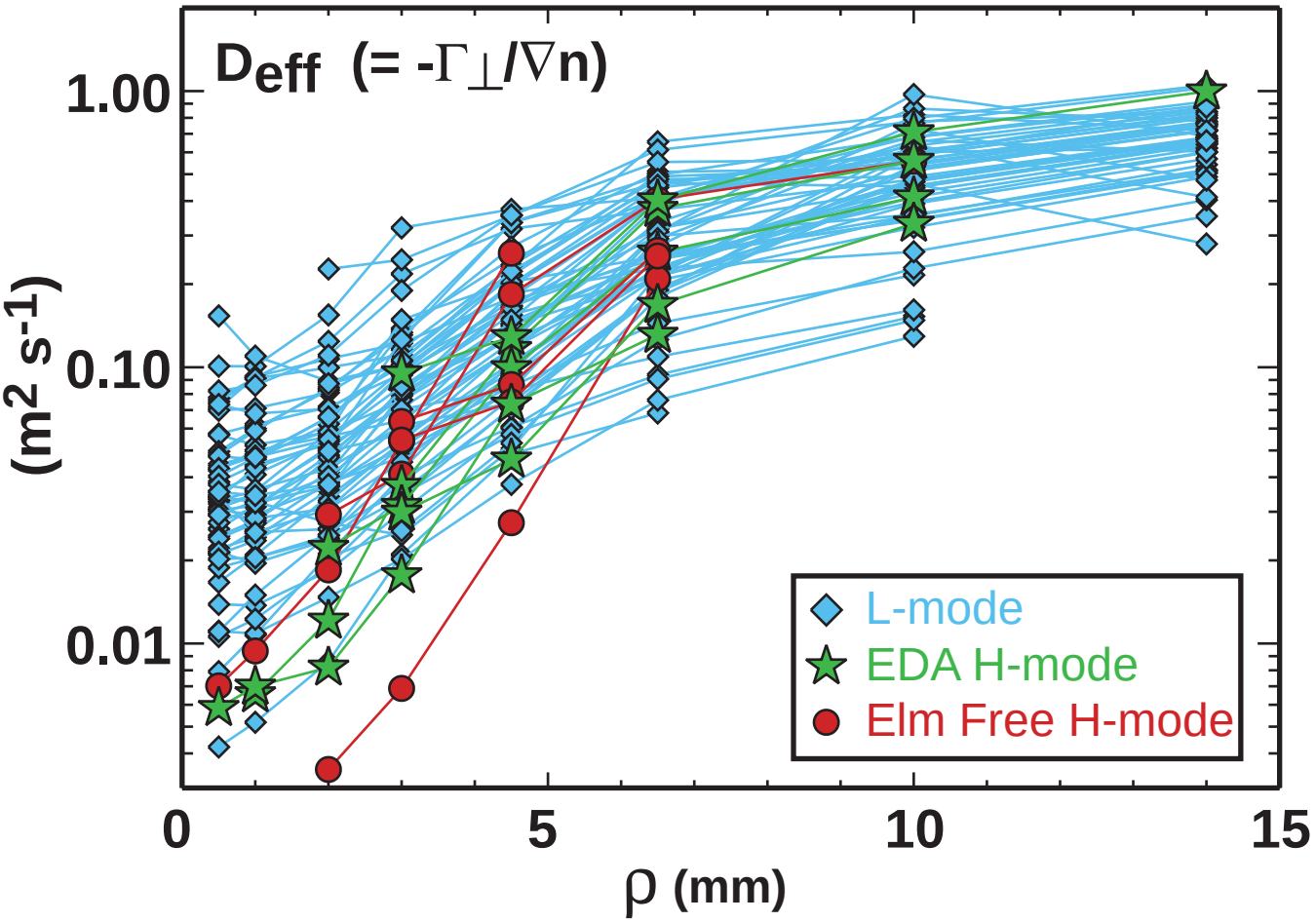


*Fig. 14. Effective cross-field particle diffusivity profiles (75 total) for ohmic L-mode discharges spanning a range of plasma density ($1.0 \times 10^{20}$ $m^{-3}$ < $\bar{n}_e$ < $2.3 \times 10^{20}$ $m^{-3}$) and a few ohmic H-mode discharges. Divertor/wall flux parameter is fixed at* $\alpha$=0.5.

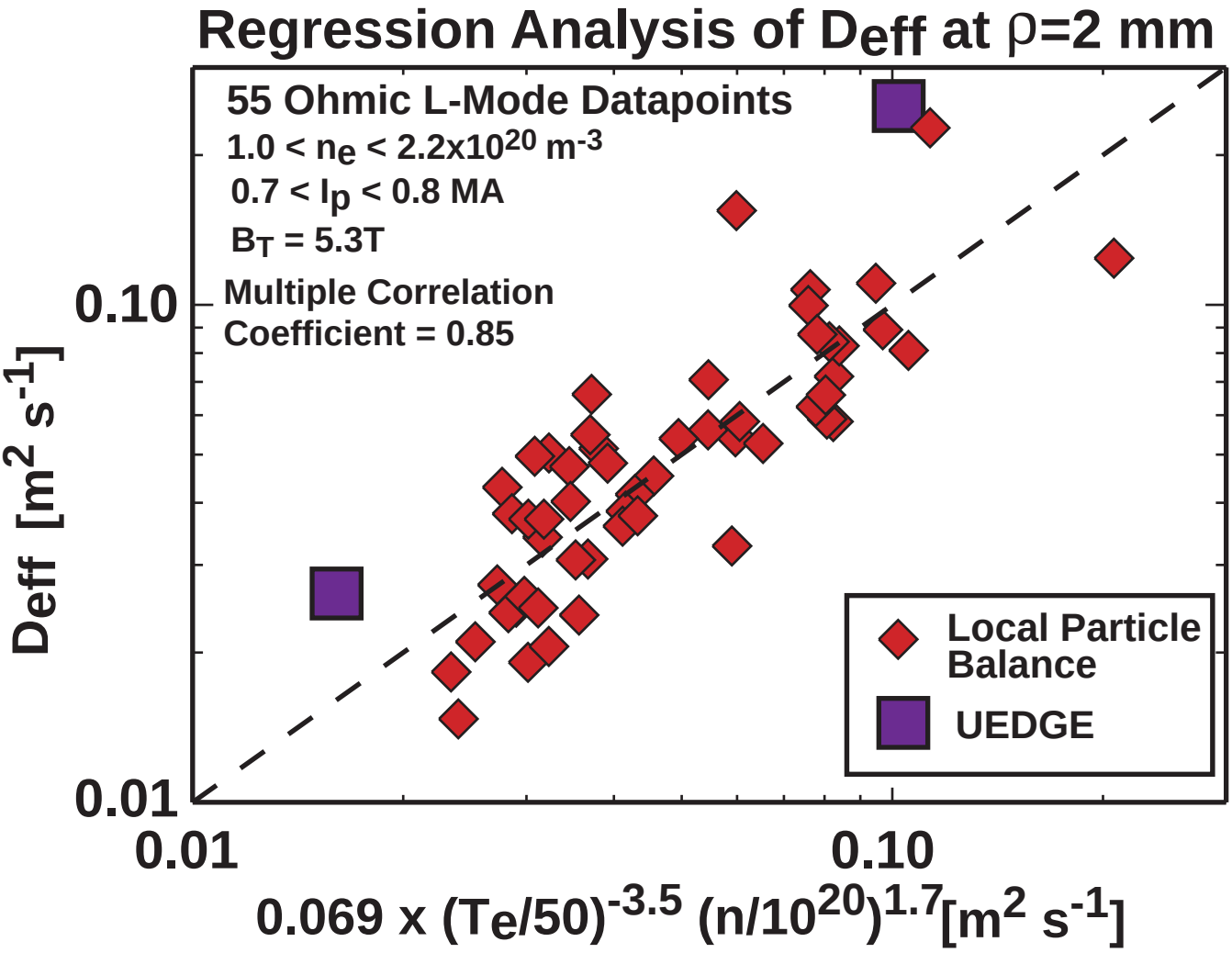


*Fig. 15. Results from regression analysis correlating local value of $D_{eff}$ (◆, inferred from direct measurement technique) with local values of electron temperature ($T_e$) and density (n) on the ρ = 2 mm flux surface. Values of $D_{eff}$ from UEDGE simulations are shown for comparison (□).*

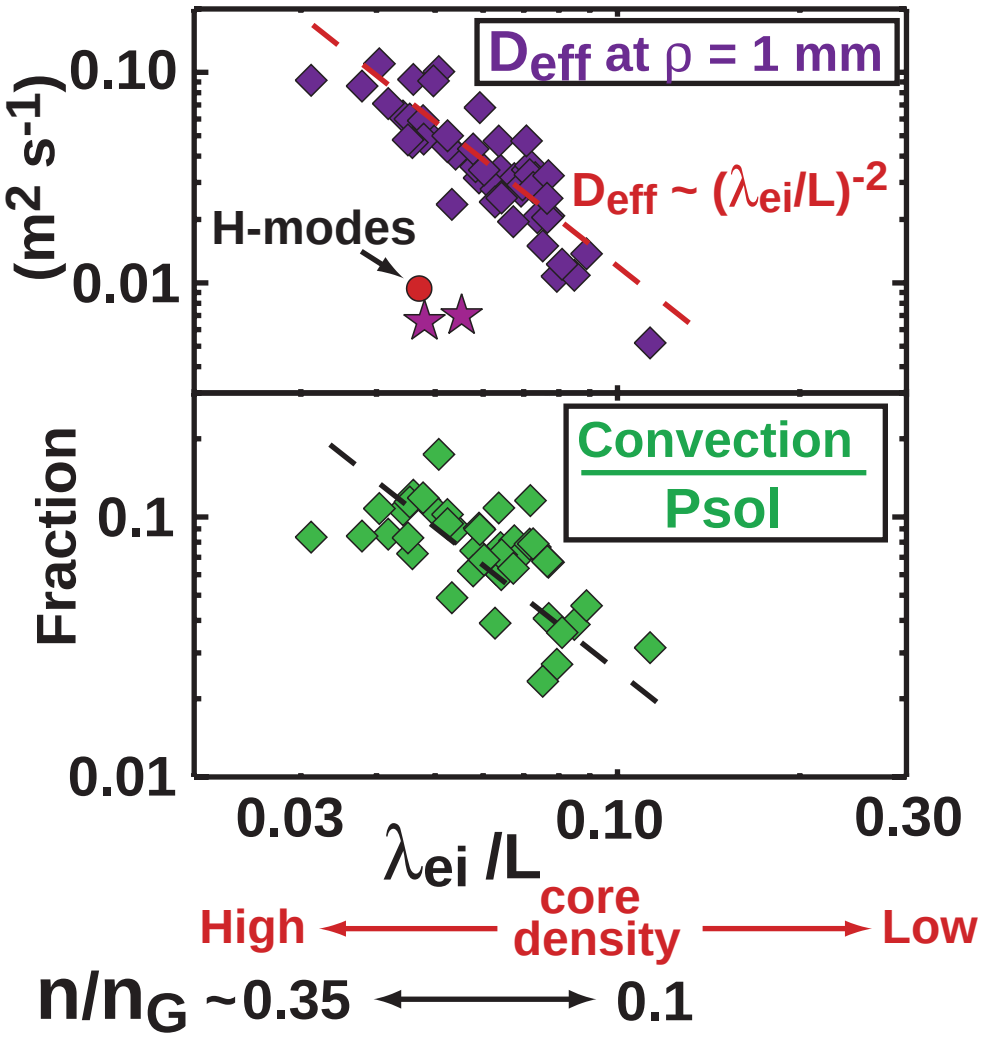


*Fig. 16. $D_{eff}$ at ρ = 1 mm flux surface location (top panel) and estimate of fraction of heat convected into SOL at ρ = 1 mm flux surface (bottom panel) versus $\lambda_{ei}/L$, the local electron mean-free path normalized to 1/2 parallel connection length. The convected component of the SOL heat flux increases sharply as $\lambda_{ei}/L$ decreases, corresponding to an increase the core plasma (n) normalized to the Greenwald density ($n_G$).*